Cell

Resource

An *in vitro* system to silence mitochondrial gene expression

Graphical abstract

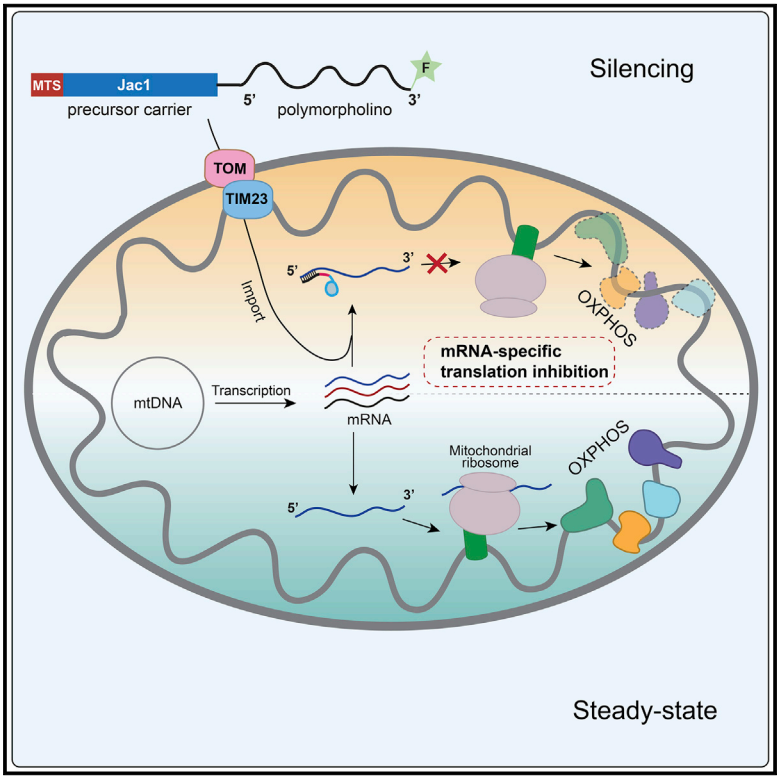

Authors

Luis Daniel Cruz-Zaragoza, Sven Dennerlein, Andreas Linden, ..., Ricarda Richter-Dennerlein, Henning Urlaub, Peter Rehling

Correspondence

peter.rehling@medizin.uni-goettingen.de

In brief

The mitochondrial genome encodes core subunits of the OXPHOS system. Imported precursor-morpholino chimera efficiently blocks the translation of mitochondrial mRNAs. Translation of bicistronic mRNAs was shown to depend on translation of the upstream open reading frame. IGF2BP1 represents a mitochondrial RNA- and ribosome-interacting protein required for mitochondrial translation.

Highlights

- Precursor-morpholino chimera can be imported into mitochondria *in vitro*
- Translation of individual mRNAs can be efficiently blocked
- Translation of bicistronic mRNAs requires translation of upstream open reading frame
- Cytosolic IGF2BP1 also localizes to mitochondria and is required for translation

Cruz-Zaragoza et al., 2021, Cell *184*, 5824–5837
November 11, 2021
https://doi.org/10.1016/j.cell.2021.09.033

CellPress

CellPress
OPEN ACCESS

Cell

Resource

An *in vitro* system to silence mitochondrial gene expression

Luis Daniel Cruz-Zaragoza,[1] Sven Dennerlein,[1] Andreas Linden,[2,3] Roya Yousefi,[1] Elena Lavdovskaia,[1,5] Abhishek Aich,[1,5] Rebecca R. Falk,[4] Ridhima Gomkale,[1] Thomas Schöndorf,[1] Markus T. Bohnsack,[4,5] Ricarda Richter-Dennerlein,[1,5] Henning Urlaub,[2,3] and Peter Rehling[1,5,6,7,*]

[1]Department of Cellular Biochemistry, University Medical Center Göttingen, 37073 Göttingen, Germany
[2]Bioanalytical Mass Spectrometry Group, Max Planck Institute for Biophysical Chemistry, Göttingen, Germany
[3]Department of Clinical Chemistry, University Medical Center Göttingen, 37073 Göttingen, Germany
[4]Department of Molecular Biology, University Medical Center Göttingen, 37073 Göttingen, Germany
[5]Cluster of Excellence, Multiscale Bioimaging: from Molecular Machines to Networks of Excitable Cells (MBExC), University of Göttingen, Göttingen, Germany
[6]Max Planck Institute for Biophysical Chemistry, 37077 Göttingen, Germany
[7]Lead contact
*Correspondence: peter.rehling@medizin.uni-goettingen.de
https://doi.org/10.1016/j.cell.2021.09.033

SUMMARY

The human mitochondrial genome encodes thirteen core subunits of the oxidative phosphorylation system, and defects in mitochondrial gene expression lead to severe neuromuscular disorders. However, the mechanisms of mitochondrial gene expression remain poorly understood due to a lack of experimental approaches to analyze these processes. Here, we present an *in vitro* system to silence translation in purified mitochondria. *In vitro* import of chemically synthesized precursor-morpholino hybrids allows us to target translation of individual mitochondrial mRNAs. By applying this approach, we conclude that the bicistronic, overlapping *ATP8/ATP6* transcript is translated through a single ribosome/mRNA engagement. We show that recruitment of COX1 assembly factors to translating ribosomes depends on nascent chain formation. By defining mRNA-specific interactomes for *COX1* and *COX2*, we reveal an unexpected function of the cytosolic oncofetal IGF2BP1, an RNA-binding protein, in mitochondrial translation. Our data provide insight into mitochondrial translation and innovative strategies to investigate mitochondrial gene expression.

INTRODUCTION

Mitochondria shape their proteome through the import of nuclear-encoded proteins and expression of their own genome. The mitochondrial genome encodes thirteen core subunits of the oxidative phosphorylation (OXPHOS) system in the inner mitochondrial membrane that converts energy from reduction equivalents into ATP. Mitochondrial gene expression requires transcription of the mitochondrial genome into two polycistronic transcripts by the mitochondrial RNA (mRNA) polymerase POLRMT. The primary transcripts are processed to form eleven mRNAs, two rRNAs, and 22 tRNAs. Two of the transcripts, *ATP8/ATP6* and *ND4L/ND4*, are bicistronic. mtPAP, the mitochondrial poly(A) polymerase, mediates polyadenylation of mRNAs (Hällberg and Larsson, 2014; Pearce et al., 2017). These maturation steps are thought to occur at defined foci termed "mitochondrial RNA granules," which also harbor stages of ribosome maturation and RNA turnover (Antonicka and Shoubridge, 2015; Pearce et al., 2017). After processing, mitochondrial mRNAs are translated by membrane-associated mitochondrial ribosomes that enable co-translational insertion of synthesized polypeptide chains into the lipid bilayer. For this, ribosomes are bound to the conserved OXA1L insertase in the membrane (Itoh et al., 2021; Ott et al., 2016; Richter-Dennerlein et al., 2015). The newly synthesized mitochondrial-encoded proteins have to associate with assembly factors in the inner membrane, which stabilize these polypeptides and maintain them competent to receive cofactors and imported, nuclear-encoded OXPHOS complex subunits. To balance mitochondrial translation with the availability of nuclear-encoded subunits, translation responds to the influx of these proteins (Couvillion et al., 2016; Richter-Dennerlein et al., 2016). Stalled ribosome nascent chain complexes seem to play a key role in this regulatory process, but the mechanisms underlying mitochondrial translation regulation remain open (Mai et al., 2017; Pearce et al., 2017; Richter-Dennerlein et al., 2016).

Considering the importance of OXPHOS for cellular function, it is not surprising that defects at every step of the mitochondrial gene expression process have been linked to human disorders (Brischigliaro and Zeviani, 2021; Fontanesi and Barrientos, 2013). Most of the patients display neuromuscular pathologies, which have been attributed to the especially high energy

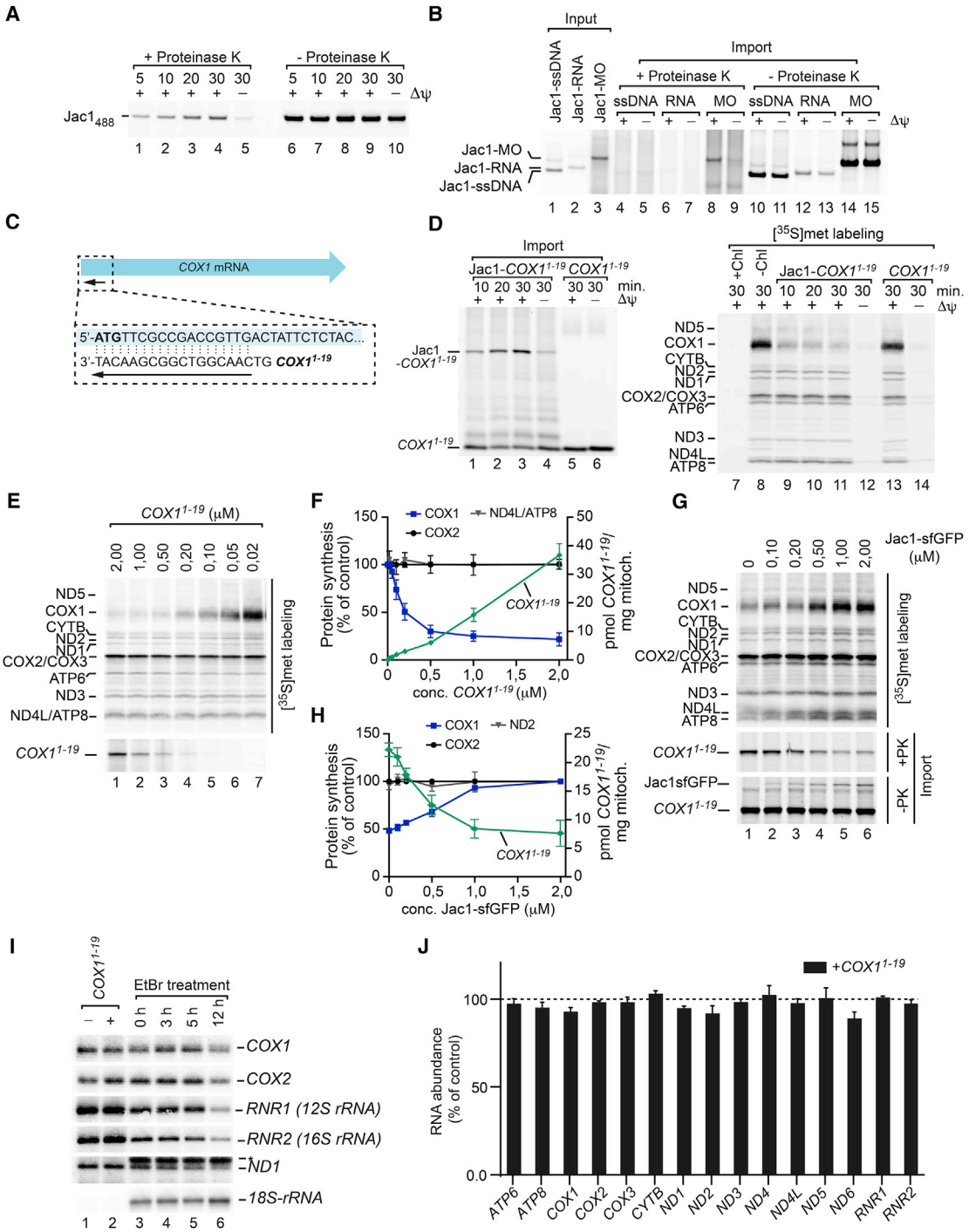

Figure 1. Experimental setup targeting COX1 translation

(A) Jac1 (coupled to DyLight488) was imported into isolated HEK293T mitochondria and treated or not with proteinase K. Δψ, membrane potential.

(B) Synthesized Jac1-hybrids with ssDNA, RNA, and polymorpholine oligonucleotides (MOs) were imported into purified HEK293T mitochondria. Non-imported adducts were removed by proteinase K treatment (lanes 4–9).

(C) Schematic presentation of morpholino-*COX1*$^{1-19}$ hybrid targeting the 5′ region of the *COX1* mRNA.

(D) *COX1*$^{1-19}$ was imported for indicated times into purified mitochondria, and a non-coupled MO was used as control. After import, mitochondria were re-isolated and subjected to *in vitro* translation in the presence of [^{35}S]methionine, and newly synthesized polypeptides were analyzed by SDS-PAGE followed by digital autoradiography (lanes 7–14). As a control, one sample was treated with chloramphenicol (Chl).

(E) Titration of the *COX1*$^{1-19}$ inhibitory effect on mitochondrial translation as in (D).

(legend continued on next page)

demands of these tissues. Nevertheless, basic principles of mitochondrial gene expression are still not understood. While recent structural analyses of mitochondrial POLRMT (Hillen et al., 2017a, 2017b) and ribosomes (Amunts et al., 2015; Greber et al., 2015; Itoh et al., 2021) provide us with insight into the machineries of gene expression, we still lack understanding of the mechanisms of these processes and how gene expression is integrated into the cellular and mitochondrial contexts. A lack of appropriate techniques to target the individual steps of gene expression represents a major obstacle to advancing our understanding. A major problem in the development of new strategies is the transport of RNAs into mitochondria that would allow us to target mitochondrial RNAs and thereby interfere with gene expression processes.

Here, we present an *in vitro* approach to target translation of mitochondrial mRNAs. Chemically synthesized protein-morpholino chimera, which are imported into purified mitochondria, allow us to specifically stall translation of selected mRNAs. Utilizing this strategy, we show that ribosome association to protein-specific assembly factors in the inner membrane occurs through nascent chain translation intermediates. In addition, we investigated the mechanism of translation of the bicistronic, overlapping *ATP8/ATP6* mRNA. Our findings indicate that a single ribosome/RNA encounter mediates expression of ATP8 and ATP6. Silencing translation of individual mRNAs allowed us to define early assembly intermediates of the OXPHOS system. Lastly, purification of chimera-associated mRNAs enabled us to define mRNA-specific interactomes and identified the cytosolic RNA-binding IGF2BP1 as an unidentified mitochondrial protein that interacts with mitochondrial ribosomes and mRNAs to regulate mitochondrial translation.

RESULTS

Targeting COX1 translation in purified mitochondria

A lack of experimental access to analyze the different steps of mitochondrial gene expression hampers our mechanistic understanding. Hence, we set out to develop an *in vitro* system to target mitochondrial translation by importing synthetic oligonucleotides. For this, we expressed and purified the mitochondrial DnaJ-homolog Jac1. Jac1 was chosen for its small size, its simple fold, its good solubility, and the fact that it contains a single cysteine (Ciesielski et al., 2012). For our analyses, we generated a C145A mutant version with a cysteine added to the C terminus. Purified Jac1 was modified with DyLight488-maleimide, generating Jac1-DyLight488 ($Jac1_{488}$) (Figures S1A and S1C). Fluorescently labeled Jac1 was efficiently imported into purified HEK293T mitochondria and displayed proteinase K resistance in the presence of a membrane potential ($\Delta\psi$) (Figure 1A). Although Jac1 contains a presequence that is removed upon import into yeast mitochondria (Voisine et al., 2001), $Jac1_{488}$ or [^{35}S]-labeled Jac1 (Figures 1A and S1B) was not efficiently processed upon import into HEK293T mitochondria. Furthermore, we addressed whether Jac1 could be used as a carrier for small nucleic acid molecules. For this, a dibenzocyclooctyne group (DBCO) was added to Jac1 by modifying the thiol group with sulfo-DBCO-PEG_4-maleimide (Figures S1A and S1C). In a subsequent click reaction, Jac1-DBCO was covalently linked to an azide group present in fluorescently labeled single-stranded DNA (ssDNA), RNA oligonucleotides, and morpholino phosphorodiamidate oligonucleotides (MO) (Figure 1B, lanes 1–3; Figures S1A, S1D, and S1E). We addressed if these Jac1-oligonucleotide chimeras were competent for import into purified mitochondria. All adducts associated with purified human mitochondria and apparently bound to the outer membrane, where they displayed protease sensitivity (Figure 1B). The amounts of protease-resistant, imported Jac1-ssDNA and Jac1-RNA were minimal at best (Figure 1B, lanes 4–7), suggesting poor import or fast turnover of the protein-nucleic acid chimera in mitochondria. In contrast, the Jac1-morpholino hybrid (Jac1-MO) was efficiently imported into mitochondria in a $\Delta\psi$-dependent manner (Figure 1B, lanes 8 and 9). Since morpholinos are relatively stable molecules and established tools to impair RNA maturation and translation through an antisense mechanism of action in the cytosol (Summerton et al., 1997; Taylor et al., 1996), we designed a morpholino targeting the 5′ end of the mitochondrial *COX1 mRNA* ($COX1^{1\text{-}19}$) (Figure 1C). To test whether Jac1-$COX1^{1\text{-}19}$ chimera could influence translation of *COX1* mRNA, we imported the purified adduct into isolated mitochondria. Jac1-$COX1^{1\text{-}19}$ was efficiently imported in a $\Delta\psi$-dependent manner (Figure 1D, lanes 1–6). After the import reaction, mitochondria were re-isolated and subjected to [^{35}S]methionine labeling of mitochondrial translation products. COX1 translation was selectively reduced in Jac1-$COX1^{1\text{-}19}$ import samples (Figure 1D, lanes 8–11). Incubation of mitochondria with free $COX1^{1\text{-}19}$ morpholino did not affect COX1 translation (Figure 1D, lanes 5, 6, and 13). The block of mitochondrial translation upon $\Delta\psi$ depletion was in agreement with previous studies (Côté et al., 1990). Apparently, the observed COX1 translation inhibition correlated with the amount of imported Jac1-$COX1^{1\text{-}19}$. To substantiate this interpretation, we titrated the amount of Jac1-$COX1^{1\text{-}19}$ (from now on referred to as $COX1^{1\text{-}19}$) in the import reactions and quantified the imported $COX1^{1\text{-}19}$ and newly translated COX1 (Figures 1E and 1F). Maximal inhibition was apparent

(F) Quantification of newly synthesized mitochondrial proteins and $COX1^{1\text{-}19}$ after $COX1^{1\text{-}19}$ import. The amount of imported $COX1^{1\text{-}19}$ was estimated based on fluorescence intensity (mean ± SEM; n = 3).

(G) The presequence import pathway was blocked by preincubation of purified mitochondria with increasing concentrations of a presequence-containing precursor fused to a tightly folded domain (Jac1-sfGFP). Subsequently, $COX1^{1\text{-}19}$ (2 μM) was imported prior to [^{35}S]methionine labeling of translation products. Jac1sfGFP and $COX1^{1\text{-}19}$ were detected by fluorescence imaging with an FITC filter.

(H) Quantification of newly synthesized mitochondrial proteins and $COX1^{1\text{-}19}$ upon Jac1-sfGFP accumulation and $COX1^{1\text{-}19}$ import as in (D) (mean ± SEM; n = 3).

(I and J) Mitochondrial RNA abundance was assessed by northern blot (I) and nanoString (J) analyses upon $COX1^{1\text{-}19}$ import (mean ± SEM; n = 3). RNA extracted from ethidium bromide-treated HEK293T cells was used as the control in northern blot analyses. RNA levels (J) are displayed as ratios of target to wild-type (WT) control (dashed line).

See also Figure S1.

with highest chimera concentration in the import reaction (2 μM), but lower concentrations of 1–0.5 μM were still effective in inhibiting COX1 translation. After we determined the effective amount, imported *COX1*$^{1-19}$, based on its fluorescence intensity, allowed us to define the IC_{50} of *COX1*$^{1-19}$ for inhibition of COX1 translation as ~2 pmol/mg mitochondria.

To corroborate that the effect of *COX1*$^{1-19}$ on mitochondrial translation was specific to imported *COX1*$^{1-19}$, purified mitochondria were incubated with increasing amounts of a chemically purified precursor with a tightly folded C-terminal domain, Jac1-sfGFP (Gomkale et al., 2021), which blocks the presequence import pathway through accumulation in the TOM/TIM23 complexes (Figure S1F). After Jac1-sfGFP accumulation, re-isolated mitochondria were subjected to *COX1*$^{1-19}$ import and [^{35}S]methionine labeling of translation products. As expected, Jac1-sfGFP accumulation blocked *COX1*$^{1-19}$ import in a dose-dependent manner and thereby rescued the mitochondrial translation from the inhibitory effect of the chimera (Figures 1G and 1H). Thus, *COX1*$^{1-19}$ was translocated into mitochondria via the TIM23 import pathway. Concomitantly, the reduction of *COX1*$^{1-19}$ import attenuated the inhibitory effect on COX1 synthesis without affecting translation of other proteins (Figures 1G and 1H).

To assess if the effect of *COX1*$^{1-19}$ on COX1 translation was due to destabilization of the *COX1* mRNA, mitochondrial RNA levels were determined in *COX1*$^{1-19}$-treated and -untreated mitochondria. Northern blot analyses did not indicate a reduction in *COX1*, *COX2*, *ND1* mRNAs, or the mitochondrial ribosomal RNAs (*RNR1* and *RNR2*, 12S and 16S rRNAs) (Figure 1I, lanes 1 and 2). As a control, we purified total RNA from HEK293T cells treated with ethidium bromide (EtBr) (Figure 1I, lanes 3–6). EtBr interferes with mitochondrial DNA replication and transcription, leading to a reduction in mitochondrial RNA abundance. In a complementary approach, we analyzed mitochondrial RNA abundance by nanoString with a previously established TagSet panel (Richter-Dennerlein et al., 2016). Also, in these analyses, neither the *COX1* mRNA nor other mitochondrial RNAs were affected by *COX1*$^{1-19}$ treatment (Figure 1J). Moreover, when mitochondrial ribosomes were purified from mitochondria (with uL1m^{FLAG} used as bait), we found a specific reduction in *COX1* mRNA association upon treatment with *COX1*$^{1-19}$ (Figure S2D). This suggests that chimera binding to the target mRNA interferes with its recognition and binding by the ribosome. In summary, we established a method to regulate COX1 translation. Precursor-morpholino chimera targeting the *COX1* mRNA could be imported into mitochondria *in vitro* and selectively inhibited translation of COX1 with high efficiency.

Dissecting early steps of COX1 biogenesis

COX1 is the mitochondrial-encoded headstone subunit of cytochrome *c* oxidase (complex IV). Loss of COX1 leads to complex IV deficiency, as apparent in several mitochondrial disorder patients (Brischigliaro and Zeviani, 2021; Fontanesi and Barrientos, 2013; Shoubridge, 2001; Weraarpachai et al., 2009, 2012). OXA1L inserts COX1 co-translationally into the membrane. A stalled ribosome-nascent chain complex of COX1 associates with early assembly factors C12ORF62 (COX14) and MITRAC12 (COA3) and imported structural subunits. This elongation stalled state allows adaptation of COX1 translation to the influx of imported proteins (Richter-Dennerlein et al., 2016) (Figure 2A). Subsequently, COX1 forms metastable assembly intermediates with diverse assembly factors and structural subunits termed MITRAC complexes that can be resolved by Blue Native (BN) PAGE analyses as a population of complexes migrating around 150 kDa in size. Targeting COX1 translation with *COX1*$^{1-19}$ *in vitro* allowed us now to address COX1 assembly with high temporal resolution and specificity, thereby avoiding indirect effects on other mitochondrial proteins. Upon *COX1*$^{1-19}$-mediated inhibition of COX1 translation, we radiolabeled mitochondrial translation products. Solubilized mitochondrial protein complexes were subsequently analyzed in a first-dimension BN-PAGE and second-dimension SDS-PAGE. Immunodetection of proteins from different OXPHOS complexes showed that, in the time frame of the treatment, neither protein stability nor complex abundance were indirectly affected (Figures 2B, S2A, and S2B). The same was true for newly synthesized mitochondrial-encoded proteins, except for COX1. While radiolabeled COX1 co-migrated with the MITRAC components C12ORF62 and MITRAC12 in untreated control mitochondria, this intermediate was lost when COX1 translation was blocked with *COX1*$^{1-19}$ (Figure 2B). The fact that MITRAC intermediates were present at steady state, despite inhibition of COX1 translation, is in line with the idea of a reservoir of COX1 in MITRAC that can be recruited for assembly of the complex (Mick et al., 2012). Thus, the time frame of the *in vitro* system allowed us to analyze COX1 translation under conditions that do not impact the assembly of complex IV at large.

A central unanswered question is how COX1-translating ribosomes are targeted to specific assembly factors in the inner mitochondrial membrane. To address this, we blocked translation of *COX1* mRNA with *COX1*$^{1-19}$ in mitochondria purified from cells expressing C12ORF62^{FLAG}. Immunoisolation of C12ORF62^{FLAG} after radiolabeling of mitochondrial translation products revealed translation intermediates in the untreated control (Richter-Dennerlein et al., 2016) that were lacking in the *COX1*$^{1-19}$-treated sample. Thus, *COX1*$^{1-19}$ efficiently prevented formation of ribosome nascent chain complexes translating COX1 (Figure 2C). In agreement with the observed presence of MITRAC complexes at steady state (Figure 2B), the amount of co-isolated MITRAC constituents OXA1L, MITRAC12, COX4-1, and TIM21 was not affected when COX1 translation was blocked *in vitro*. In contrast, ribosome association to C12ORF62 was drastically reduced when COX1 translation was blocked (Figure 2D). We also determined the amounts of mitochondrial RNAs in the immunoisolated fractions. *RNR1* (12S rRNA, mtSSU), *RNR2* (16S rRNA, mtLSU), and the *COX1* mRNA co-isolated with C12ORF62 (Figure 2E). However, treatment with *COX1*$^{1-19}$ and the concomitant block in translation of COX1 strongly affected the association of the *COX1* mRNA and mitochondrial rRNA with C12ORF62 (Figure 2E and inset). Accordingly, COX1 translation is a prerequisite for ribosome association to the transcript-specific assembly factor C12ORF62. Apparently, formation of a COX1 nascent chain facilitates association with early MITRAC complexes. In a complementary approach, the mitochondrial ribosome was immunoisolated via mL45^{FLAG}. While C12ORF62

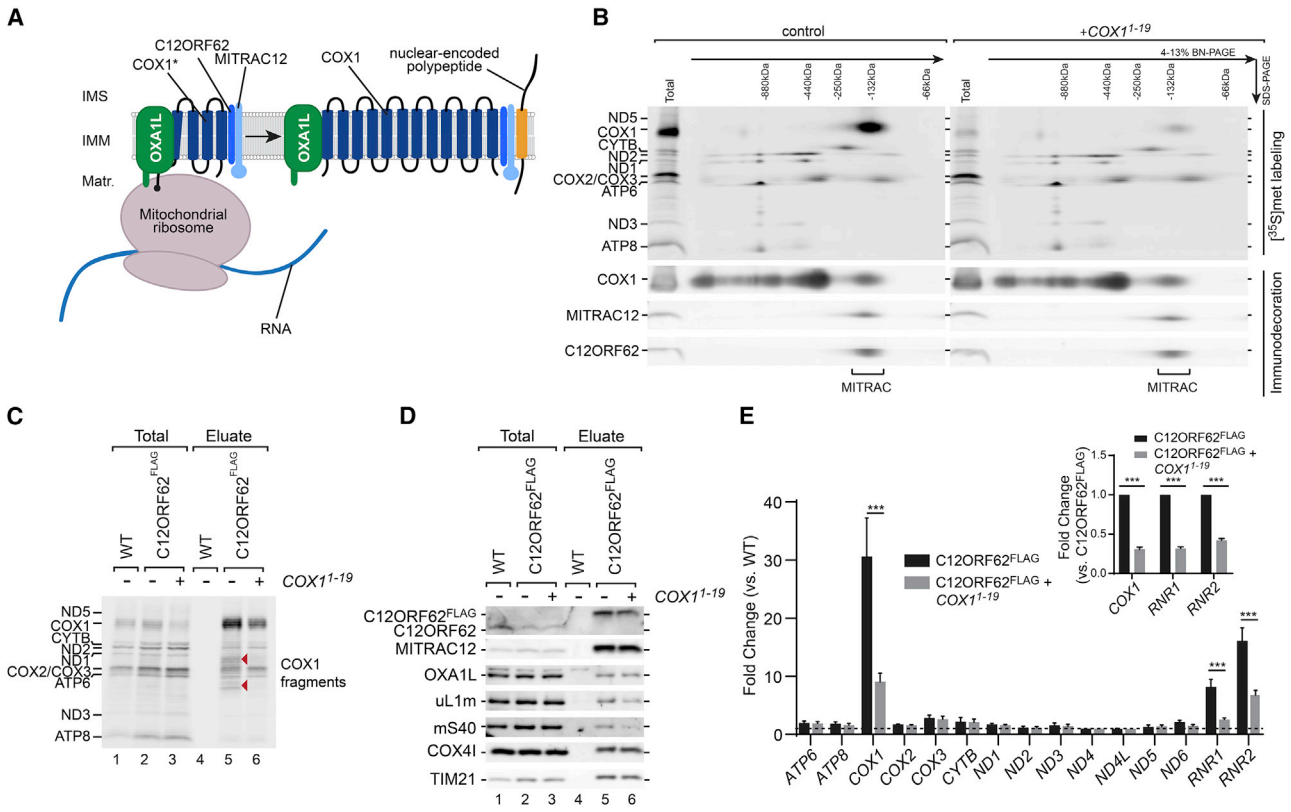

Figure 2. MITRAC-associated ribosomes are actively translating COX1

(A) Schematic presentation of early stages of COX1 biogenesis.

(B) After blocking COX1 synthesis, mitochondria were solubilized and protein complexes analyzed by 2D-BN/SDS-PAGE followed by digital autoradiography or immunodecoration.

(C) C12ORF62^{FLAG} was immunoisolated from purified mitochondria after *COX1*$^{1-19}$ import and [^{35}S]methionine labeling of translation products. Stalled COX1 translation intermediates are highlighted with red arrows.

(D) C12ORF62^{FLAG} was immunopurified from mitochondria after *COX1*$^{1-19}$-mediated block in COX1 translation. Samples were analyzed by western blotting (total, 5%; eluate, 100%).

(E) Mitochondrial RNAs co-isolated by C12ORF62^{FLAG} immunoisolation in (D) were quantified by nanoString technology. Enrichment of selected RNAs is displayed as the ratio between sample and control (WT, dashed line). *COX1* mRNA, *RNR1*, and *RNR2* association to MITRAC upon COX1 translation downregulation are presented as a ratio to the untreated sample in the inset (mean ± SEM; n = 3).

See also Figure S2.

was co-precipitated from the untreated sample, treatment with *COX1*$^{1-19}$ drastically decreased its ribosome association (Figure S2C). Based on this, we conclude at the inner membrane, *COX1* mRNA and the ribosomal subunits are recycled from early assembly factors after translation.

Targeting translation of OXPHOS subunits

Four complexes of the OXPHOS system contain mitochondrial-encoded subunits: ND1, ND2, ND3, ND4, ND4L, ND5, and ND6 in complex I; CYTB in complex III; COX1, COX2, and COX3 in complex IV; and ATP8 and ATP6 in complex V (Figure 3A). To test if translation of all of the corresponding mRNAs could be blocked *in vitro*, we designed antisense morpholinos (Figure S3A) that were coupled to the Jac1-protein carrier (Figure S3B). The protein-morpholino chimeras were imported into purified mitochondria and protein synthesis addressed by [^{35}S]methionine labeling. Translation products were analyzed by SDS-PAGE (Figure 3) and first-dimension BN-PAGE followed by second-dimension SDS-PAGE (Figures S4 and S5) to visualize protein complexes containing the newly synthesized translation products. Treatment with *CYTB*$^{6-24}$ specifically reduced CYTB translation and led to loss of a 250 kDa complex III assembly intermediate (Figures 3B and S5B). In the case of complex IV, in addition to COX1 (see above), COX2 and COX3 synthesis could be specifically blocked by morpholinos (Figures 3C,S5D, and S5E). We asked if the *in vitro* system to target mitochondrial translation in human mitochondria could be applied to mitochondria from a different origin. Since mice are broadly used to model human mitochondrial diseases, morpholinos were designed against mouse *COX1* and *CYTB* mRNA. Carrier protein-morpholino chimeras of *mCOX1*$^{1-24}$ and *mCYTB*$^{2-24}$ were imported into mitochondria purified from mice brain, followed by *in vitro* translation. The treatment resulted in the block of translation of COX1 and CYTB (Figure 3D).

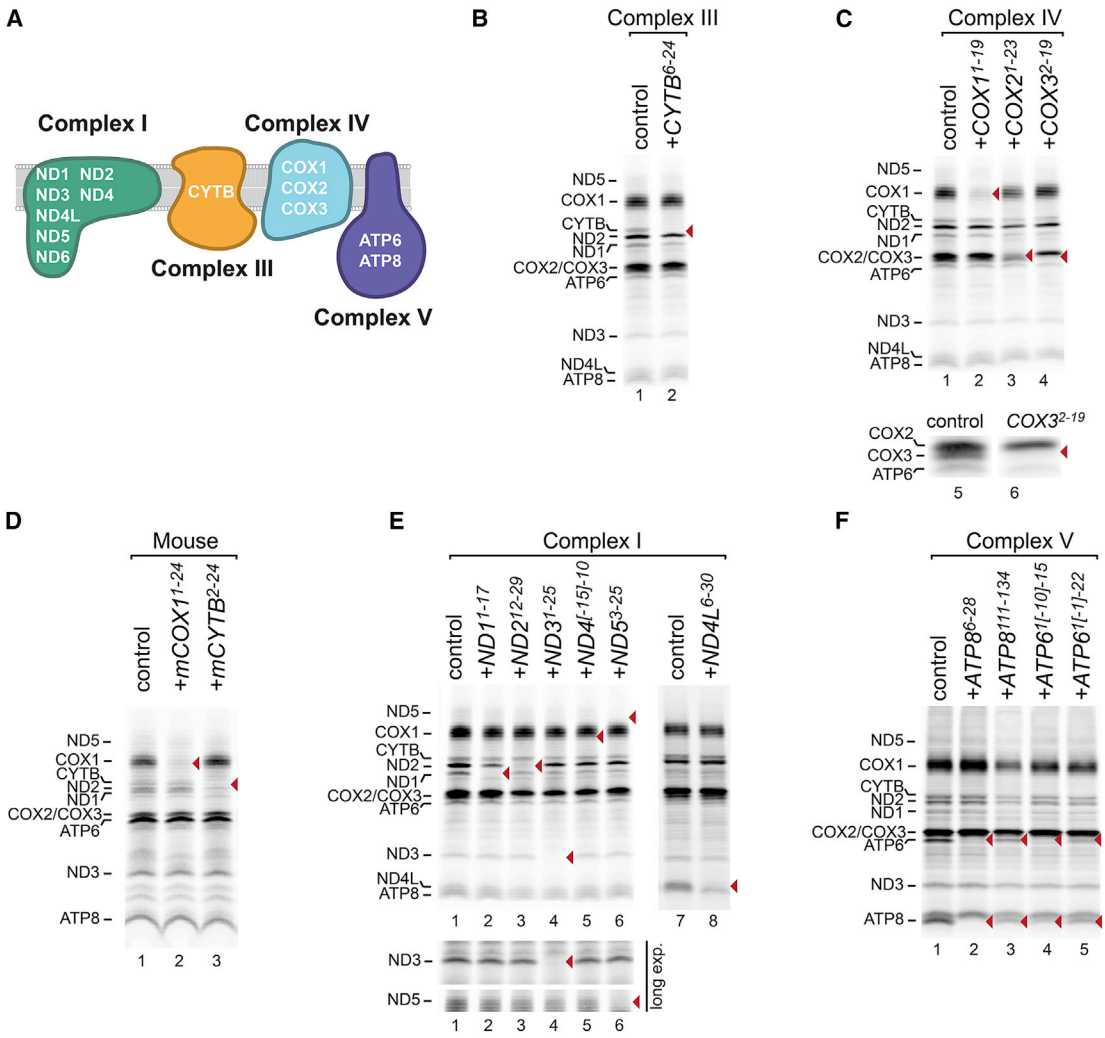

Figure 3. Targeting mRNA translation in human and mice mitochondria

(A) Schematic presentation of mitochondrial-encoded proteins in complexes of the OXPHOS system.

(B and C) Indicated mRNAs encoding subunits of complex III (B) and complex IV (C) were targeted by importing morpholinos into purified human mitochondria. Subsequently, mitochondrial translation products were radiolabeled and analyzed by SDS-PAGE and digital autoradiography. The targeted binding site into the referred mRNA codon is indicated in superscript.

(D) Precursor-morpholino chimeras targeting complex III (*mCYTB*$^{2-24}$) and complex IV (*mCOX1*$^{1-24}$) were imported into isolated mouse brain mitochondria prior to radiolabeling of translation products.

(E) Targeting complex I subunits synthesis in purified human mitochondria as described in (B) and (C).

(F) Bicistronic *ATP8/ATP6* RNA was targeted with morpholino probes binding to the 5′ end of both ORFs and internally in *ATP8*. Purified mitochondria were subjected to precursor-morpholino chimera import and [^{35}S]methionine labeling of translation products. Newly synthesized polypeptides were analyzed by SDS-PAGE and digital autoradiography.

Relevant bands are indicated in each case.

See also Figures S3, S4, and S5.

In the case of complex I subunits ND1, ND2, ND3, and ND5, the translation products were well resolved by SDS-PAGE (Figures 3E and S4); ND4L and ND4, which migrate close to ATP8 and COX1, respectively, were visualized by 2D-PAGE (Figures 3E, S4E, and S4F). Translation of ND1, ND2, ND3, ND4L, ND4, and ND5 was efficiently blocked by imported chimera. When comparing complex formation by BN-PAGE, newly synthesized ND1, ND2, ND3, and ND4L co-migrated with complexes of more than 440 kDa. Interestingly, ND1-5 proteins co-migrated as part of complexes larger than 880 kDa, suggesting their assembly into mature complex I (approximately 970 kDa) (Figure S4A) (Guerrero-Castillo et al., 2017). Interestingly, blocking ND1 translation led to reduction of ND2 levels (45.2% ± 7.2% of control) (Figure 3E). In contrast, blocking ND2 translation did not affect ND1 levels (Figure 3E). Considering that ND1 and ND2 are thought to initially assemble into different modules (Guerrero-Castillo et al., 2017; Stroud et al., 2016), this observation was unexpected. Blocking translation of ND3, ND4, and ND5 did not

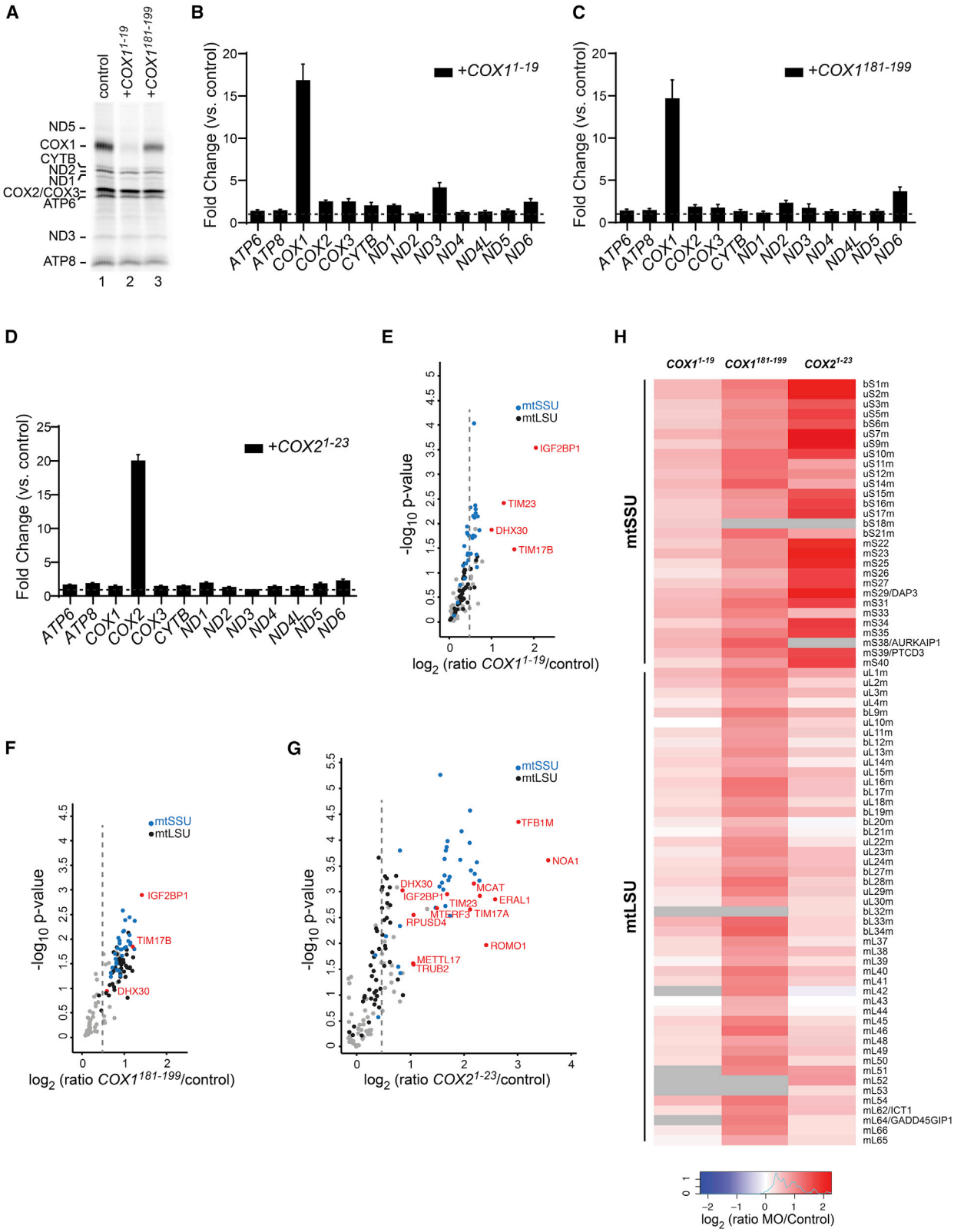

(legend on next page)

affect synthesis of other ND proteins (Figures 3E and S4). ND4L and ND4 are encoded by a bicistronic mRNA (Figure S3C). While ND4L synthesis was not altered by ND4 reduction, ND4L downregulation led to a considerable reduction in ND4 synthesis (Figures S4E and S4F).

Translational coupling of ATP8 and ATP6 synthesis

ATP6 and ATP8 are the mitochondrial-encoded subunits of complex V and participate in proton-channel formation in the F_o portion of the complex. The two proteins are translation products of a bicistronic mRNA. The open reading frames (ORFs) are partially overlapping and not in the same reading frame (Figure S3D). It is a long-standing question if translation of the two ORFs requires two independent ribosome association events or if they are translated by a single ribosome engagement with the mRNA (Hällberg and Larsson, 2014). We tested this by treating mitochondria with *ATP8*$^{6\text{-}28}$, directed against the *ATP8/ATP6* mRNA (*RNA14*) 5′ end. In addition to the expected block in ATP8 synthesis, ATP6 translation was no longer observed (Figure 3F, lane 2). Targeting the ATP6 start codon (*ATP6*$^{[-1]\text{-}22}$) caused a reduction in ATP6 and ATP8 synthesis (Figure 3F, lane 5). Moreover, *ATP6*$^{[-10]\text{-}15}$ blocked ATP6 synthesis, but ATP8 translation still occurred at a somewhat reduced level (Figure 3F, lane 4). The different effects of morpholinos targeting the ATP6 start codon (*ATP6*$^{[-1]\text{-}22}$) or the upstream region (*ATP6*$^{[-10]\text{-}15}$) indicate that expression of ATP6 requires upstream access of the translation machinery to regions in ATP8. Interestingly, ATP8 and ATP6 targeting was a non-commutative effect, suggesting that a stoichiometric expression of the two proteins could be achieved through the coupled translation process. Taken together, ATP6 synthesis depends on ATP8 translation and appears to occur through a single ribosome transcript association.

Defining mitochondrial RNA interactors

Considering the effect of the tested morpholino-chimera on translation of mitochondrial mRNAs, we addressed whether the chimera could be used to isolate target mRNAs together with interacting proteins. For this, we utilized *COX1*$^{1\text{-}19}$ and *COX2*$^{1\text{-}23}$ and also designed a second morpholino targeting COX1, *COX1*$^{181\text{-}199}$, which was complementary to an internal region in *COX1* mRNA (Figure S6A). In comparison to *COX1*$^{1\text{-}19}$, *COX1*$^{181\text{-}199}$ was slightly less effective in blocking COX1 synthesis (approximately 80% compared to control) (Figure 4A). A likely explanation is that in the presence of *COX1*$^{181\text{-}199}$, the ribosome is able to associate to the *COX1* mRNA, initiate translation, and displace *COX1*$^{181\text{-}199}$ from the transcript as reported for cytosolic ribosome (Summerton, 1999). The protein-morpholino chimeras, which contained a FLAG-tag in the protein portion, were imported into purified mitochondria. Subsequently, mitochondria were solubilized and subjected to immunoisolation, and copurifying mRNAs were analyzed by nanoString technology. The *COX1* mRNA was significantly enriched in the *COX1*$^{1\text{-}19}$ and *COX1*$^{181\text{-}199}$ samples (Figures 4B and 4C), while *COX2*$^{1\text{-}23}$ enriched specifically the *COX2* mRNA (Figure 4D). When mitochondrial ribosomes were purified via uL1m^{FLAG}, *COX1*$^{1\text{-}19}$ and *COX2*$^{1\text{-}23}$ treatment led to specifically reduced ribosome association of their cognate transcript (*COX1* mRNA, 67.8% ± 6.0% of control; *COX2* mRNA, 68.8% ± 8.0% of control) (Figures S2D and S2E).

We applied the chimera-purification regime to mitochondria isolated from cells after stable isotope labeling by amino acids in cell culture (SILAC) for a quantitative assessment of associated proteins (Figure S6B). Immunoisolations were analyzed by mass spectrometry to determine proteins specifically enriched with the chimeric bait. As a control, we utilized the Jac1^{FLAG} carrier alone (Figures 4E–4G; Table S1). In all cases, components of the mitochondrial ribosome were enriched. Moreover, we detected subunits of the TIM23 complex (TIM17A, TIM17B, TIM23, and ROMO1), likely reflecting a slower import rate of the protein-morpholino chimera. *COX2*$^{1\text{-}23}$ especially enriched mtSSU subunits. In addition, we identified factors involved in mitochondrial RNA maturation and ribosome assembly (RPSUD4, TRUB2, NOA1, ERAL1, and TFB1M). However, in the case of *COX1*$^{181\text{-}199}$, mtSSU and mtLSU subunits copurified with similar efficiency (Figure 4H). Accordingly, binding of the *COX2*$^{1\text{-}23}$ morpholino to the target mRNA 5′ end might still allow mtSSU association to the RNA but appears to impair binding of the mtLSU for monosome formation. Interestingly, TACO1 (translational activator of cytochrome *c* oxidase 1) protein was not identified among the interactors isolated with COX1 chimeras.

IGF2BP1 is required for mitochondrial translation

In addition to ribosomal proteins, we identified three proteins that were co-isolated with *COX1* and *COX2* mRNAs (Figures 5A and 5B). The presence of the insertase OXA1L indicated that a fraction of isolated mRNA/ribosome complexes were membrane-associated and primed to protein insertion. In addition, DHX30, a mitochondrial ATP-dependent RNA helicase, and IGF2 mRNA-binding protein 1 (IGF2BP1), a cytosolic mRNA-binding protein, were identified in all three isolations and their presence confirmed by immunodetection (Figure 5C).

Figure 4. Identification of mitochondrial mRNA-associated proteins

(A) Precursor-morpholino adducts directed against *COX1* 5′ terminus (*COX1*$^{1\text{-}19}$) or internally (*COX1*$^{181\text{-}199}$) were imported into purified mitochondria prior to radiolabeling and analysis of mitochondrial translation products by SDS-PAGE and digital autoradiography.

(B–D) Purified mitochondria from SILAC-labeled HEK293T were subjected to import of *COX1*$^{1\text{-}19}$ (B), *COX1*$^{181\text{-}199}$ (C), *COX2*$^{1\text{-}23}$ (D), or non-conjugated precursor protein (control) followed by FLAG-immunoisolation of the Jac1 precursor. RNA was isolated from eluates and analyzed by nanoString technology (mean ± SEM; n = 4).

(E–G) Eluates were subjected to mass-spectrometric analyses (n = 4). Results are presented as volcano plots for *COX1*$^{1\text{-}19}$ (E), *COX1*$^{181\text{-}199}$ (F), and *COX2*$^{1\text{-}23}$ (G). The threshold for $\log_2$ (mean ratio) > 0.5 is shown as a dashed line. Components of the large subunit (mtLSU) and small subunit (mtSSU) of the mitochondrial ribosome are presented in black and blue, respectively. Selected proteins are indicated in red.

(H) Heatmap of the detected mtLSU and mtSSU proteins in (E)–(G). Color intensity correlates to the $\log_2$ (mean ratio) as defined in the legend.

See also Figure S6 and Table S1.

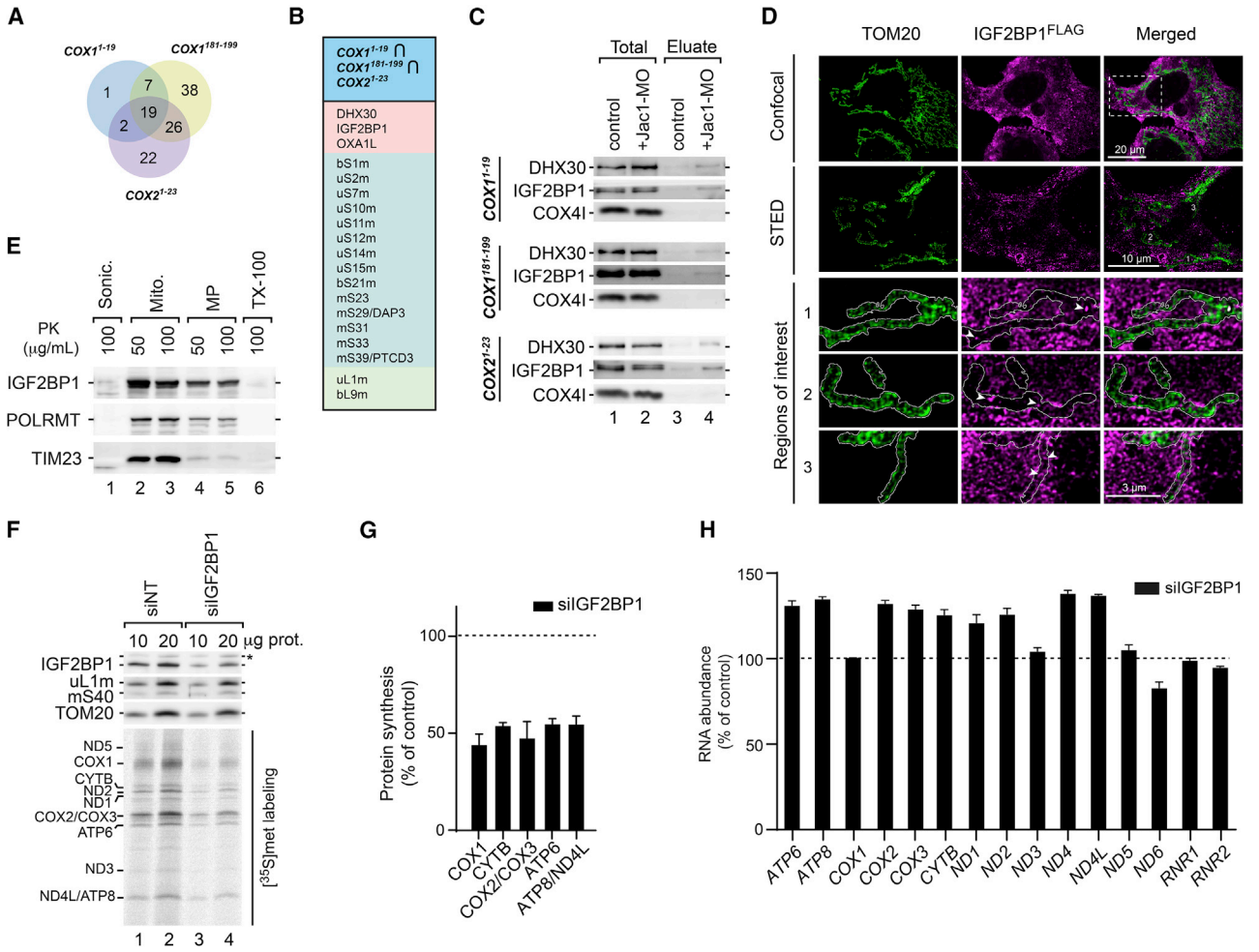

Figure 5. Loss of IGF2BP1 affects mitochondrial protein translation

(A) Venn diagram after grouping of proteins enriched in Figures 4F–4H with $\log_2$ (mean ratio) > 0.5.

(B) List of overlapping proteins identified the three-group intersection in (A). Structural subunits of mtLSU (green), mtSSU (light blue), and non-ribosomal proteins (red).

(C) After import into purified mitochondria, indicated Jac1-morpholino chimera were immunoisolated from mitochondria and analyzed by western blotting for the presence of DHX30 and IGF2BP1. Total, 5%; eluate 100%.

(D) Immunofluorescence confocal and STED microscopy of cells expressing IGF2BP1^{FLAG}. IGF2BP1 was detected with an anti-FLAG antibody, and TOM20 was used as a mitochondrial marker. Regions of interest (ROIs) indicated appear magnified. Arrowheads indicate IGF2BP1 foci localized into the mitochondrial matrix.

(E) Purified intact (Mito.), swollen (MP, mitoplast), detergent-lysed (TX-100), and sonicated (Sonic.) mitochondria were subjected to proteinase K treatment and analyzed by western blotting to determine the submitochondrial localization of IGF2BP1.

(F) Mitochondrial translation products were labeled with [^{35}S]methionine after siRNA-mediated downregulation of IGF2BP1 in HEK293T cells. Control, non-targeting siRNA (siNT).

(G) Quantification of [^{35}S]methionine-labeled mitochondrial translation products from (F), compared to siNT control (mean ± SEM; n = 3).

(H) RNA abundance was determined by nanoString technology in mitochondria from IGF2BP1-depleted cells and compared to siNT control (dashed line) (mean ± SEM; n = 3).

See also Figure S6.

DHX30 was previously shown to display dual localization to the cytoplasm and the mitochondrial matrix (Antonicka and Shoubridge, 2015; Lessel et al., 2017). However, IGF2BP1 was defined as a cytosolic protein with a role in mRNA stabilization (Nielsen et al., 1999; Weidensdorfer et al., 2009). To this end, we addressed the subcellular localization of IGF2BP1 by fluorescence microscopy, utilizing a C-terminally tagged version of IGF2BP1 (IGF2BP1^{FLAG}). We confirmed the cytosolic localization of the protein (Figure 5D). However, STED microscopic analyses showed that a fraction of IGF2BP1 co-localized with the mitochondrial marker TOM20 (Figure 5D). Protease protection analyses were performed to determine the sub-mitochondrial localization of the authentic IGF2BP1. IGF2BP1 behaved similarly to the mitochondrial matrix protein POLRMT, further supporting a matrix localization of a fraction of the cellular IGF2BP1 (Figure 5E).

IGF2BP1 associates to cytosolic transcripts to regulate their stability and translation (Nielsen et al., 1999; Stöhr et al., 2006; Weidensdorfer et al., 2009). We therefore tested if a loss of IGF2BP1 affected mitochondrial translation. Applying small interfering RNA (siRNA)-mediated knockdown of IGF2BP1, we radiolabeled mitochondrial translation products. Despite incomplete depletion of IGF2BP1, mitochondrial translation efficiency was significantly reduced (Figures 5F and 5G). Similarly, the loss of DHX30 led to a mitochondrial translation defect (Figures S6C and S6D). In both cases, the levels of tested mitochondrial ribosomes were not affected by the siRNA treatment (Figures 5F and S6C). Quantification of the newly synthesized mitochondrial proteins showed a general translation phenotype (Figures 5G and S6D). Thus, IGF2BP1 and DHX30 did not display transcript-specific phenotypes but instead affected the translation of all transcripts.

The broad effect on mitochondrial mRNA translation led us to determine if the loss of IGF2BP1 or DHX30 affected steady-state levels of mitochondrial mRNAs. Compared to the control mitochondria, depletion of IGF2BP1 did not cause reduction of mitochondrial mRNAs, and even a slight increase in mRNA levels was apparent (Figure 5H). In contrast, DHX30 depletion led to a partial reduction of few of the transcripts including *RNR1* and *RNR2* (Figure S6E).

In summary, purification of imported chimeras allowed identification of mRNA-associated proteins. In addition to the previously identified helicase DHX30 and OXA1L insertase, we recovered the cytosolic RNA-interacting IGF2BP1 protein. A fraction of IGF2BP1 localizes to the mitochondrial matrix and is required for translation of mitochondrial mRNAs.

IGF2BP1 associates with mitochondrial ribosomes

Since depletion of IGF2BP1 did not limit mRNA abundance in mitochondria, we addressed if IGF2BP1 interacted with mitochondrial ribosomes. Mitochondria from IGF2BP1^{FLAG}-expressing cells were subjected to FLAG immunoisolation analyses. Both mtLSU (uL1m and uL10m) and mtSSU (uS14m) co-isolated with IGF2BP1 (Figure 6A). In agreement, *RNR1* and *RNR2* were enriched in the IGF2BP1 immunoprecipitate (Figure 6B). Using the same strategy, we also demonstrated that DHX30 associated with mitochondrial ribosomes (Figures S6F and S6G). Moreover, IGF2BP1 was found associated to a different extent with mitochondrial mRNAs encoding especially complexes IV and V subunits and, to a lesser extent, complex I (Figure 6C). In contrast, DHX30 displayed association to complex IV- and I-encoding transcripts and ribosomal RNAs (Figures S6G and S6H).

As DHX30 was previously suggested to participate in mitochondrial ribosome assembly (Antonicka and Shoubridge, 2015), we tested if downregulation of IGF2BP1 affected ribosome biogenesis. To this end, under conditions of IGF2BP1 or DHX30 depletion, we purified ribosomes via uL1m^{FLAG}. In both cases, subunits of the small ribosomal subunit were efficiently co-isolated with uL1m^{FLAG} (Figures 6D and S6I). Moreover, sucrose density gradient analyses of mitochondria lysates depleted for IGF2BP1 or DHX30 were performed to separate mtLSU (39S), mtSSU (28S), and the monosome (55S). These analyses did not indicate altered ribosome assembly in the absence of IGF2BP1 or DHX30 (Figures 6E and S6J). Accordingly, translation defects observed under conditions of IGF2BP1 or DHX30 knockdown cannot be attributed to defects in ribosome formation but rather to a role of these proteins in priming mitochondrial mRNAs for translation.

Two paralogs of IGF2BP1, IGF2BP2 and IGF2BP3, have been identified as mRNA-binding protein family members (reviewed in Degrauwe et al., 2016). Because all three proteins cooperate and were implicated in the formation of ribonucleoprotein granules (Jønson et al., 2007), we investigated whether IGF2BP2 and IGF2BP3 similarly co-isolated with the mitochondrial ribosome. When ribosomes were immunoisolated from mitochondria by uL1^{FLAG}, IGF2BP1, −2, and −3 were recovered in the eluate (Figure 6F). Accordingly, the three cytosolic IGF2BP-family members display dual localization to the cytosol and mitochondria. Considering that IGF2BP2 has been implicated in expression of mRNAs encoding nuclear-encoded OXPHOS subunits (Janiszewska et al., 2012), our results suggest that this protein family impacts OXPHOS biogenesis by regulating nuclear- and mitochondrial-genome encoded transcripts of OXPHOS subunits.

DISCUSSION

For understanding molecular mechanisms, reductionist approaches are essential tools that allow us to dissect biological processes and the function of components involved. Our understanding of mitochondrial gene expression is limited by the lack of such approaches that would allow us to interfere with the processes at any level. A major obstacle to develop experimental strategies lies in the fact that mitochondria are not readily genetically accessible (Lightowlers, 2011; Patananan et al., 2016). At the cellular level, modified DNA can be introduced into mitochondria of yeast by particle bombardment (Bonnefoy and Fox, 2007; Johnston et al., 1988). Yet this technique cannot be applied to higher eukaryotic mitochondria. In human cells, mitochondria DNA could recently be modified by expressing an engineered cytidine deaminase mediating C/G to T/A conversions (Mok et al., 2020). The apparent lack of *in vitro* approaches to target gene expression is largely due to the fact that oligonucleotides cannot be efficiently delivered to mitochondria (Vestweber and Schatz, 1989) to bind or interfere with mitochondrial transcripts. To tackle this, we have developed a technique that allows us to target translation in purified mitochondria. By using chimera of a mitochondrial precursor protein chemically linked to a morpholino, which targets specific transcripts, we were able to interfere with the translation of individual organellar mRNAs. These chimeras are imported efficiently into purified mitochondria, and picomolar concentrations were sufficient to block translation of the targeted mRNA molecule. This *in vitro* system allows us to investigate how the loss of expression of an individual mRNA affects mitochondrial physiology and organization in a time range of minutes with minimal indirect effects on other processes. While most of our analysis was carried out with human mitochondria, the technique was easily transferred to purified mice mitochondria, indicating applicability also in the context of disease models.

In proof-of-principle analyses, we targeted mitochondrial mRNAs to address the biology of mitochondrial gene expression.

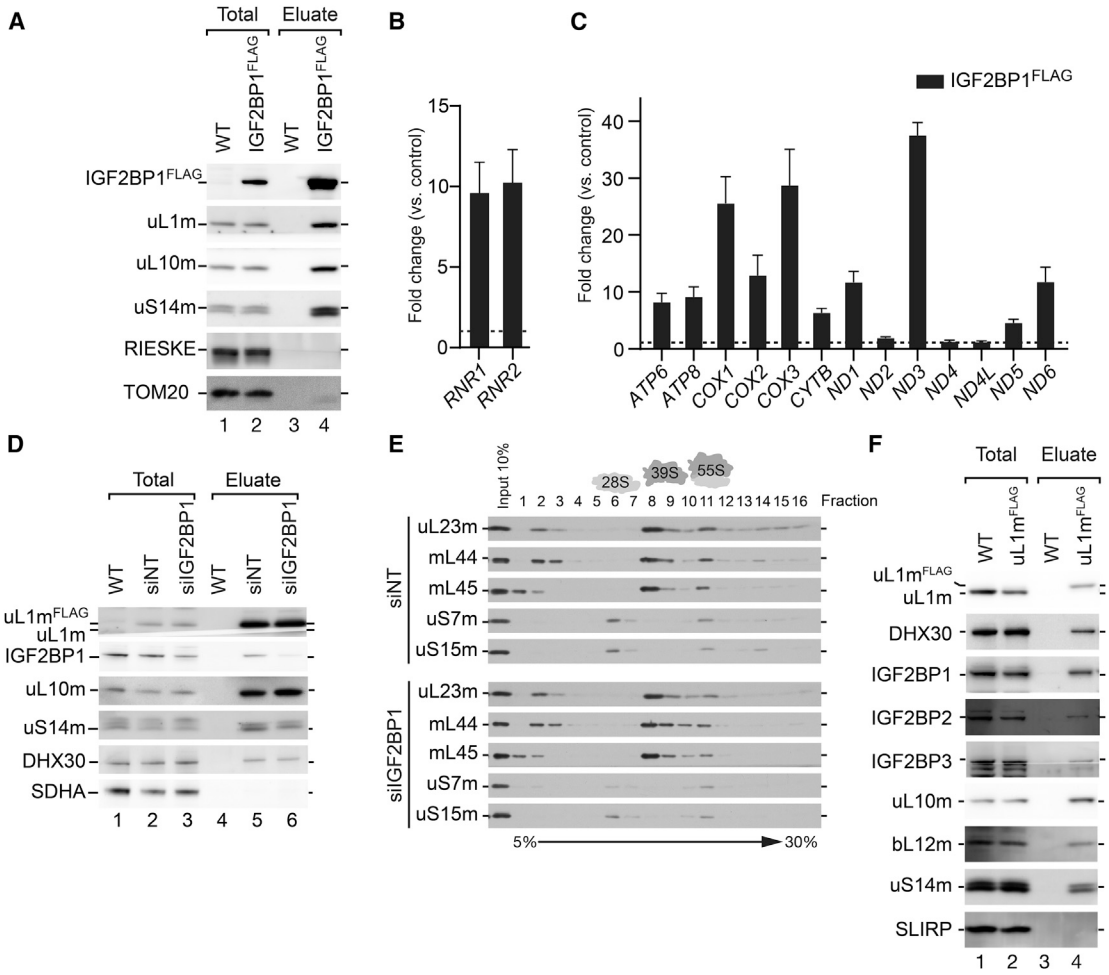

Figure 6. IGF2BP1 associates with the mitochondrial ribosome

(A) IGF2BP1^{FLAG} was immunoisolated from mitochondria purified from HEK293T cells. Samples were analyzed by western blotting. Total, 3%; eluate, 100%.

(B) Mitochondrial rRNA abundance in eluates from (A) was analyzed by nanoString technology and is presented as fold change to the WT control (dashed line) (mean ± SEM; n = 3).

(C) Mitochondrial mRNA abundance in eluates from (A) was analyzed by nanoString technology. The results are presented as fold change to the WT control (dashed line) (mean ± SEM; n = 3).

(D) Mitochondrial ribosomes were isolated from purified mitochondria after siRNA-mediated downregulation of IGF2BP1 via uL1m^{FLAG} immunoisolation. Samples were analyzed by western blotting. Total, 3%; eluate, 100%.

(E) Mitochondrial extracts from control (siNT) and IGF2BP1-depleted HEK293T cells were subjected to sucrose density gradient analyses to separate mtSSU (28S), mtLSU (39S), and monosome (55S).

(F) Ribosomes were immunoisolated via uL1m^{FLAG} from purified mitochondria. Samples were analyzed by western blotting. Total, 3%; eluate, 100%.

See also Figure S6.

Mitochondrial ribosomes associate to the membrane, where OXA1L inserts nascent polypeptides into the lipid phase. During this process, translation-product-specific assembly factors associate to the ribosome nascent chain complex (Richter-Dennerlein et al., 2015). It is unresolved at what stage of translation ribosomes are bound by OXA1L and how early assembly factors are recruited to the insertion complex. By studying the COX1 assembly factor C12ORF62, we could show that a block in *COX1* translation affects ribosome binding to C12ORF62 without affecting association between C12ORF62 and OXA1L. Apparently, association of early assembly factors with the ribosome depends on the formation of a ribosome nascent chain complex, suggesting that the recruitment of the assembly factor occurs through the translation product. It is tempting to speculate that a COX1-independent association between OXA1L and C12ORF62 indicates that dedicated insertase complexes that are primed to receive ribosomes exist in the membrane. This conclusion implies that after translation, ribosomes would not remain bound to assembly factors but rather dissociate to make them available to a new round of co-translational protein insertion.

The bicistronic transcripts *ATP8* and *ATP6* represent overlapping ORFs. Whether a single ribosome mRNA engagement facilitates expression of both proteins is a long-standing question (Gao et al., 2017; Hällberg and Larsson, 2014). Our analyses

showed that translation of *ATP6* depends on translation of the upstream localized *ATP8*. This result is in agreement with a single ribosome-mRNA engagement, which allows translation of the ATP8 transcript first and subsequently translation of ATP6. Such a scenario would suggest that, after translation of *ATP8* has been completed, the ribosomes would have to move backward in order to reinitiate translation of *ATP6*. An alternative explanation could be that a proposed hairpin-loop region between *ATP8* and *ATP6* (Venkata Subbaiah et al., 2019) doesn't allow for ribosome binding upstream of the *ATP6* transcript unless structural reorganization of the transcript occurs in the context of *ATP8* translation. However, it will be challenging to ultimately exclude any of the two possibilities. Interestingly, the second mitochondrial bicistronic RNA, *ND4L/ND4* mRNA, also showed a similar behavior; ND4 translation depends on the translation of the upstream-localized ND4L.

The availability of mRNA-specific chimeras allowed us to purify their target mRNAs and associated proteins. Our analyses on *COX1* and *COX2* mRNAs identified the helicase DHX30 as the binding protein of these transcripts. Previous analyses of DHX30 indicated binding to ribosomal RNAs and a broad range of mitochondrial mRNAs. The observed translation defects in the absence of DHX30 were attributed to a role of DHX30 in the biogenesis of mitochondrial ribosomes (Antonicka and Shoubridge, 2015). Our study similarly showed a broad range of mRNA targets for DHX30 but with a more pronounced interaction with *ND3* and *ND6* transcripts than seen by Antonicka and Shoubridge. Using the nanoString technology, we did not observe a significant increase in abundance for any mitochondrial transcript in the absence of DHX30. Moreover, under our 72 h knockdown conditions, a ribosome assembly defect was not apparent. We concluded that DHX30 interacts with mitochondrial RNAs but that an effect on mitochondrial ribosome assembly can only be observed after longer knockdown and thus might represent an indirect effect. As a translation defect was detected by us under conditions when ribosome abundance and assembly were not affected and DHX30 was found to be ribosome associated, we conclude that DHX30 participates in mitochondrial translation in a more direct manner.

A surprising finding in our analyses was the identification of IGF2BP1 as an interactor with mitochondrial RNAs. Insulin-like growth factor 2 (IGF2) mRNA-binding protein 1 (IGF2BP1) belongs to a conserved family of cytoplasmic RNA-binding proteins that consists of three members in mammals (IGF2BP1-3), also termed IMP1-3. These three proteins have been found to regulate cytoplasmic RNA stability, processing, localization, and translation (Degrauwe et al., 2016). During mammalian embryogenesis, IMP1-3 are expressed in most organs and apparently involved in regulating metabolism and stem cell renewal. However, in adult tissues, IGF2BP2 appears to be the mainly expressed paralog, yet the IMPs have been found to be re-expressed and active under conditions of malignant transformation in cancer. Here we showed that a fraction of IGF2BP1 localizes to the mitochondrial matrix. It remains open as to how IGF2BP1 is targeted to the mitochondrial matrix as no presequence could be predicted. However, unidentified internal signals in the polypeptide chain might be able to direct the protein into the matrix. In the matrix of mitochondria, IGF2BP1 interacts with mitochondrial ribosomes and mRNAs. In agreement with this, knockdown of IGF2BP1 affects mitochondrial translation without impacting the abundance and assembly state of mitochondrial ribosomes. We could show that in addition to IGF2BP1, IGF2BP2 and −3 are associated with the mitochondrial ribosome. Interestingly, IGF2BP2 has been found to regulate OXPHOS in primary glioblastoma through an interaction with nuclear-encoded mitochondrial transcripts (Janiszewska et al., 2012). Accordingly, IGF2BPs appear to be able to modulate cellular metabolism not only through interactions with nuclear transcripts but also in mitochondria to promote expression of the organellar genome.

Our data show that this *in vitro* system to target mitochondrial gene expression at the level of translation provides a powerful approach to dissect the mechanism of translation but also the biology of mitochondrial transcripts at large.

Limitations of the study

The *in vitro* system described here relies on the import of precursor-morpholino chimeras into purified mitochondria via the presequence import pathway. Thus, defects in mitochondrial physiology that impact the import pathway would interfere with the silencing strategy. Accordingly, mitochondrial fitness is important for the experimental approach. The strategy aims to address questions with minimal indirect effect as short-term effects are analyzed. However, purified mitochondria cannot be maintained active for prolonged periods of time, and therefore the time frame of the silencing reaction is limited. Despite these considerations, the *in vitro* silencing strategy described here serves as a means to tackle mechanistic questions regarding mitochondrial gene expression in a transcript-specific manner with high temporal resolution.

STAR★METHODS

Detailed methods are provided in the online version of this paper and include the following:

- KEY RESOURCES TABLE
- RESOURCE AVAILABILITY
  - Lead contact
  - Materials availability
  - Data and code availability
- EXPERIMENTAL MODEL AND SUBJECT DETAILS
  - Human-derived cell lines culture
  - Bacterial culture
  - Yeast culture
- METHOD DETAILS
  - Recombinant Jac1 expression and purification
  - Synthesis of $Jac1_{488}$, Jac1-DBCO, and Jac1-oligonucleotide chimera
  - Cell culture
  - *In vivo* [^{35}S] methionine labeling of mitochondrial translation products
  - siRNA-mediated protein knockdown
  - $IGF2BP1^{FLAG}$ transient expression in HEK293T
  - Isolation of mitochondria from HEK293T cells
  - Isolation of mitochondria from *Saccharomyces cerevisiae* cells

- Import of $Jac1_{488}$ into HEK293T mitochondria
- Import of [^{35}S]Jac1 into *Saccharomyces cerevisiae* and HEK293T mitochondria
- Import of Jac1-oligonucleotide chimera into human mitochondria
- Downregulation of mtDNA-encoded genes by Jac1-morpholino chimera in human mitochondria
- Titrating the effect of imported Jac1-$COX1^{1-19}$ on mitochondrial translation
- Blocking the presequnce import pathway with Jac1-sfGFP prior Jac1-$COX1^{1-19}$ import
- Downregulation of mtDNA-encoded genes by Jac1-morpholino chimera in mouse brain mitochondria
- Native immunoprecipitation of FLAG-tagged proteins
- Protease protection assay
- Mitochondrial RNA detection by nanoString technology
- Protein electrophoresis and immunodetection
- Northern blot
- Mitochondria isolation and sucrose density gradient ultracentrifugation
- LC-MS/MS analysis
- Volcano plot and heatmap preparation
- Immunostaining for confocal and STED microscopy
- Image acquisition

● QUANTIFICATION AND STATISTICAL ANALYSIS

SUPPLEMENTAL INFORMATION

Supplemental information can be found online at https://doi.org/10.1016/j.cell.2021.09.033.

ACKNOWLEDGMENTS

We would like to thank past and present members of the Rehling laboratory for support and discussion. We thank K.E. Bohnsack, N. Tautz, and M. Rodnina for discussion and O. Bernhard and M. Wissel for expert technical assistance. Funded by the Deutsche Forschungsgemeinschaft (DFG, German Research Foundation) under Germany's Excellence Strategy EXC 2067/1-390729940: SFB1190 (projects P08/14 [M.T.B.], P13 [P.R.], and Z02 [H.U.]), SFB860 (B01 [P.R.]), and SFB1286 (A06 [P.R.]); DFG Emmy Noether grant (RI 2715/1-1 to R.R.-D.); the Max Planck Society (P.R. and H.U.); and the PhD program Molecular Biology – International Max Planck Research School and the Göttingen Graduate School for Neurosciences and Molecular Biosciences (GGNB; DFG grant GSC 226/1) (R.G. and R.Y.).

AUTHOR CONTRIBUTIONS

L.D.C.-Z., S.D., and P.R. developed the concept of the study. L.D.C.-Z., S.D., A.L., R.Y., E.L., A.A., R.R.F., T.S., and R.G. performed the experiments. L.D.C.-Z. and P.R. wrote the original draft. L.D.C.-Z., S.D., R.R.-D., H.U., M.T.B., and P.R. reviewed and edited the final draft of the manuscript. P.R. provided supervision.

DECLARATION OF INTERESTS

The authors declare that they have no conflict of interest.

Received: May 11, 2021
Revised: September 10, 2021
Accepted: September 24, 2021
Published: October 20, 2021

REFERENCES

Amunts, A., Brown, A., Toots, J., Scheres, S.H.W., and Ramakrishnan, V. (2015). Ribosome. The structure of the human mitochondrial ribosome. Science *348*, 95–98.

Antonicka, H., and Shoubridge, E.A. (2015). Mitochondrial RNA granules are centers for posttranscriptional RNA processing and ribosome biogenesis. Cell Rep. *10*, 920–932.

Bonnefoy, N., and Fox, T.D. (2007). Directed alteration of Saccharomyces cerevisiae mitochondrial DNA by biolistic transformation and homologous recombination. In Mitochondria: Practical Protocols, D. Leister and J.M. Herrmann, eds. (Humana Press), pp. 153–166.

Brischigliaro, M., and Zeviani, M. (2021). Cytochrome c oxidase deficiency. Biochim Biophys Acta Bioenerg *1862*, 148335.

Ciesielski, S.J., Schilke, B.A., Osipiuk, J., Bigelow, L., Mulligan, R., Majewska, J., Joachimiak, A., Marszalek, J., Craig, E.A., and Dutkiewicz, R. (2012). Interaction of J-protein co-chaperone Jac1 with Fe-S scaffold Isu is indispensable in vivo and conserved in evolution. J. Mol. Biol. *417*, 1–12.

Côté, C., Poirier, J., and Boulet, D. (1989). Expression of the mammalian mitochondrial genome. Stability of mitochondrial translation products as a function of membrane potential. J. Biol. Chem. *264*, 8487–8490.

Côté, C., Boulet, D., and Poirier, J. (1990). Expression of the mammalian mitochondrial genome. Role for membrane potential in the production of mature translation products. J. Biol. Chem. *265*, 7532–7538.

Couvillion, M.T., Soto, I.C., Shipkovenska, G., and Churchman, L.S. (2016). Synchronized mitochondrial and cytosolic translation programs. Nature *533*, 499–503.

Cox, J., and Mann, M. (2008). MaxQuant enables high peptide identification rates, individualized p.p.b.-range mass accuracies and proteome-wide protein quantification. Nat. Biotechnol. *26*, 1367–1372.

Degrauwe, N., Suvà, M.-L., Janiszewska, M., Riggi, N., and Stamenkovic, I. (2016). IMPs: an RNA-binding protein family that provides a link between stem cell maintenance in normal development and cancer. Genes Dev. *30*, 2459–2474.

Fontanesi, F., and Barrientos, A. (2013). Mitochondrial cytochrome c oxidase assembly in health and human diseases. In Mitochondrial Disorders Caused by Nuclear Genes, L.-J.C. Wong, ed. (Springer New York), pp. 239–259.

Frezza, C., Cipolat, S., and Scorrano, L. (2007). Organelle isolation: functional mitochondria from mouse liver, muscle and cultured fibroblasts. Nat. Protoc. *2*, 287–295.

Gao, F., Wesolowska, M., Agami, R., Rooijers, K., Loayza-Puch, F., Lawless, C., Lightowlers, R.N., and Chrzanowska-Lightowlers, Z.M.A. (2017). Using mitoribosomal profiling to investigate human mitochondrial translation. Wellcome Open Res. *2*, 116.

Gomkale, R., Cruz-Zaragoza, L.D., Suppanz, I., Guiard, B., Montoya, J., Callegari, S., Pacheu-Grau, D., Warscheid, B., and Rehling, P. (2020). Defining the substrate spectrum of the TIM22 complex identifies pyruvate carrier subunits as unconventional cargos. Curr. Biol. *30*, 1119–1127.e5.

Gomkale, R., Linden, A., Neumann, P., Schendzielorz, A.B., Stoldt, S., Dybkov, O., Kilisch, M., Schulz, C., Cruz-Zaragoza, L.D., Schwappach, B., et al. (2021). Mapping protein interactions in the active TOM-TIM23 supercomplex. Nat. Commun. *12*, 5715.

Greber, B.J., Bieri, P., Leibundgut, M., Leitner, A., Aebersold, R., Boehringer, D., and Ban, N. (2015). Ribosome. The complete structure of the 55S mammalian mitochondrial ribosome. Science *348*, 303–308.

Guerrero-Castillo, S., Baertling, F., Kownatzki, D., Wessels, H.J., Arnold, S., Brandt, U., and Nijtmans, L. (2017). The assembly pathway of mitochondrial respiratory chain complex I. Cell Metab. *25*, 128–139.

Haag, S., Sloan, K.E., Ranjan, N., Warda, A.S., Kretschmer, J., Blessing, C., Hübner, B., Seikowski, J., Dennerlein, S., Rehling, P., et al. (2016). NSUN3 and ABH1 modify the wobble position of mt-tRNAMet to expand codon recognition in mitochondrial translation. EMBO J. *35*, 2104–2119.

Hällberg, B.M., and Larsson, N.-G. (2014). Making proteins in the powerhouse. Cell Metab. *20*, 226–240.

Hillen, H.S., Morozov, Y.I., Sarfallah, A., Temiakov, D., and Cramer, P. (2017a). Structural basis of mitochondrial transcription initiation. Cell *171*, 1072–1081.e10.

Hillen, H.S., Parshin, A.V., Agaronyan, K., Morozov, Y.I., Graber, J.J., Chernev, A., Schwinghammer, K., Urlaub, H., Anikin, M., Cramer, P., and Temiakov, D. (2017b). Mechanism of transcription anti-termination in human mitochondria. Cell *171*, 1082–1093.e13.

Itoh, Y., Andréll, J., Choi, A., Richter, U., Maiti, P., Best, R.B., Barrientos, A., Battersby, B.J., and Amunts, A. (2021). Mechanism of membrane-tethered mitochondrial protein synthesis. Science *371*, 846–849.

Janiszewska, M., Suvà, M.L., Riggi, N., Houtkooper, R.H., Auwerx, J., Clément-Schatlo, V., Radovanovic, I., Rheinbay, E., Provero, P., and Stamenkovic, I. (2012). Imp2 controls oxidative phosphorylation and is crucial for preserving glioblastoma cancer stem cells. Genes Dev. *26*, 1926–1944.

Johnston, S.A., Anziano, P.Q., Shark, K., Sanford, J.C., and Butow, R.A. (1988). Mitochondrial transformation in yeast by bombardment with microprojectiles. Science *240*, 1538–1541.

Jønson, L., Vikesaa, J., Krogh, A., Nielsen, L.K., Hansen, Tv., Borup, R., Johnsen, A.H., Christiansen, J., and Nielsen, F.C. (2007). Molecular composition of IMP1 ribonucleoprotein granules. Mol. Cell. Proteomics *6*, 798–811.

Lessel, D., Schob, C., Küry, S., Reijnders, M.R.F., Harel, T., Eldomery, M.K., Coban-Akdemir, Z., Denecke, J., Edvardson, S., Colin, E., et al.; DDD study; C4RCD Research Group (2017). *De Novo* missense mutations in *DHX30* impair global translation and cause a neurodevelopmental disorder. Am. J. Hum. Genet. *101*, 716–724.

Lightowlers, R.N. (2011). Mitochondrial transformation: time for concerted action. EMBO Rep. *12*, 480–481.

Mai, N., Chrzanowska-Lightowlers, Z.M.A., and Lightowlers, R.N. (2017). The process of mammalian mitochondrial protein synthesis. Cell Tissue Res. *367*, 5–20.

Mick, D.U., Dennerlein, S., Wiese, H., Reinhold, R., Pacheu-Grau, D., Lorenzi, I., Sasarman, F., Weraarpachai, W., Shoubridge, E.A., Warscheid, B., and Rehling, P. (2012). MITRAC links mitochondrial protein translocation to respiratory-chain assembly and translational regulation. Cell *151*, 1528–1541.

Moggridge, S., Sorensen, P.H., Morin, G.B., and Hughes, C.S. (2018). Extending the compatibility of the SP3 paramagnetic bead processing approach for proteomics. J. Proteome Res. *17*, 1730–1740.

Mok, B.Y., de Moraes, M.H., Zeng, J., Bosch, D.E., Kotrys, A.V., Raguram, A., Hsu, F., Radey, M.C., Peterson, S.B., Mootha, V.K., et al. (2020). A bacterial cytidine deaminase toxin enables CRISPR-free mitochondrial base editing. Nature *583*, 631–637.

Nielsen, J., Christiansen, J., Lykke-Andersen, J., Johnsen, A.H., Wewer, U.M., and Nielsen, F.C. (1999). A family of insulin-like growth factor II mRNA-binding proteins represses translation in late development. Mol. Cell. Biol. *19*, 1262–1270.

Ott, M., Amunts, A., and Brown, A. (2016). Organization and regulation of mitochondrial protein synthesis. Annu. Rev. Biochem. *85*, 77–101.

Patananan, A.N., Wu, T.-H., Chiou, P.-Y., and Teitell, M.A. (2016). Modifying the mitochondrial genome. Cell Metab. *23*, 785–796.

Pearce, S.F., Rebelo-Guiomar, P., D'Souza, A.R., Powell, C.A., Van Haute, L., and Minczuk, M. (2017). Regulation of mammalian mitochondrial gene expression: recent advances. Trends Biochem Sci. *42*, 625–639.

R. Development Core Team (2014). R: A Language and Environment for Statistical Computing ((R Foundation for Statistical Computing)). https://www.r-project.org/.

Richter-Dennerlein, R., Dennerlein, S., and Rehling, P. (2015). Integrating mitochondrial translation into the cellular context. Nat. Rev. Mol. Cell Biol. *16*, 586–592.

Richter-Dennerlein, R., Oeljeklaus, S., Lorenzi, I., Ronsör, C., Bareth, B., Schendzielorz, A.B., Wang, C., Warscheid, B., Rehling, P., and Dennerlein, S. (2016). Mitochondrial protein synthesis adapts to influx of nuclear-encoded protein. Cell *167*, 471–483.e10.

Shoubridge, E.A. (2001). Cytochrome c oxidase deficiency. Am. J. Med. Genet. *106*, 46–52.

Sikorski, R.S., and Hieter, P. (1989). A system of shuttle vectors and yeast host strains designed for efficient manipulation of DNA in *Saccharomyces cerevisiae*. Genetics *122*, 19–27.

Stöhr, N., Lederer, M., Reinke, C., Meyer, S., Hatzfeld, M., Singer, R.H., and Hüttelmaier, S. (2006). ZBP1 regulates mRNA stability during cellular stress. J. Cell Biol. *175*, 527–534.

Stroud, D.A., Surgenor, E.E., Formosa, L.E., Reljic, B., Frazier, A.E., Dibley, M.G., Osellame, L.D., Stait, T., Beilharz, T.H., Thorburn, D.R., et al. (2016). Accessory subunits are integral for assembly and function of human mitochondrial complex I. Nature *538*, 123–126.

Summerton, J. (1999). Morpholino antisense oligomers: the case for an RNase H-independent structural type. Biochim. Biophys. Acta. *1489*, 141–158.

Summerton, J., Stein, D., Huang, S.B., Matthews, P., Weller, D., and Partridge, M. (1997). Morpholino and phosphorothioate antisense oligomers compared in cell-free and in-cell systems. Antisense Nucleic Acid Drug Dev. *7*, 63–70.

Taylor, M.F., Paulauskis, J.D., Weller, D.D., and Kobzik, L. (1996). *In vitro* efficacy of morpholino-modified antisense oligomers directed against tumor necrosis factor-alpha mRNA. J. Biol. Chem. *271*, 17445–17452.

Tyanova, S., Temu, T., Sinitcyn, P., Carlson, A., Hein, M.Y., Geiger, T., Mann, M., and Cox, J. (2016). The Perseus computational platform for comprehensive analysis of (prote)omics data. Nat. Methods *13*, 731–740.

Venkata Subbaiah, K.C., Hedaya, O., Wu, J., Jiang, F., and Yao, P. (2019). Mammalian RNA switches: molecular rheostats in gene regulation, disease, and medicine. Comput. Struct. Biotechnol. J. *17*, 1326–1338.

Vestweber, D., and Schatz, G. (1989). DNA-protein conjugates can enter mitochondria via the protein import pathway. Nature *338*, 170–172.

Voisine, C., Cheng, Y.C., Ohlson, M., Schilke, B., Hoff, K., Beinert, H., Marszalek, J., and Craig, E.A. (2001). Jac1, a mitochondrial J-type chaperone, is involved in the biogenesis of Fe/S clusters in *Saccharomyces cerevisiae*. Proc. Natl. Acad. Sci. USA *98*, 1483–1488.

Weidensdorfer, D., Stöhr, N., Baude, A., Lederer, M., Köhn, M., Schierhorn, A., Buchmeier, S., Wahle, E., and Hüttelmaier, S. (2009). Control of c-myc mRNA stability by IGF2BP1-associated cytoplasmic RNPs. RNA *15*, 104–115.

Weraarpachai, W., Antonicka, H., Sasarman, F., Seeger, J., Schrank, B., Kolesar, J.E., Lochmüller, H., Chevrette, M., Kaufman, B.A., Horvath, R., and Shoubridge, E.A. (2009). Mutation in TACO1, encoding a translational activator of COX I, results in cytochrome c oxidase deficiency and late-onset Leigh syndrome. Nat. Genet. *41*, 833–837.

Weraarpachai, W., Sasarman, F., Nishimura, T., Antonicka, H., Auré, K., Rötig, A., Lombès, A., and Shoubridge, E.A. (2012). Mutations in *C12orf62*, a factor that couples COX I synthesis with cytochrome c oxidase assembly, cause fatal neonatal lactic acidosis. Am. J. Hum. Genet. *90*, 142–151.

STAR★METHODS

KEY RESOURCES TABLE

REAGENT or RESOURCE	SOURCE	IDENTIFIER
Antibodies		
Rabbit polyclonal anti-ATP5B	This paper	#4826
Rabbit polyclonal anti-COX1	This paper	#5120
Rabbit polyclonal anti-COX4-I	This paper	#1522
Rabbit polyclonal anti-COX6A	This paper	#3282
Rabbit polyclonal anti-C12ORF62	This paper	#4844
Rabbit polyclonal anti-DHX30	Bethyl Laboratories	Cat# A302-218A; RRID: AB_1730985
Mouse monoclonal anti-FLAG	Sigma-Aldrich	Cat# F1804; RRID: AB_262044
Rabbit polyclonal ant-IGF2BP1	Proteintech	Cat# 22803-1-AP; RRID: AB_2879173
Rabbit polyclonal anti-IGF2BP2	Proteintech	Cat# 11601-1-AP; RRID: AB_2122672
Mouse monoclonal anti-IGF2BP3	Proteintech	Cat# 66526-1-Ig; RRID: AB_2881889
Rabbit polyclonal anti-NDUFA9	This paper	#1524
Mouse monoclonal anti-OXA1L	Proteintech	Cat# 66128-1-Ig; RRID: AB_2881527
Rabbit polyclonal anti-POLRMT	Abcam	Cat# ab32988; RRID: AB_873619
Rabbit polyclonal anti-RIESKE	This paper	#1512
Mouse monoclonal anti-SDHA	ThermoFisher Scientific	Cat# 459200; RRID: AB_2532231
Rabbit polyclonal anti-SLIRP	This paper	#3762
Rabbit polyclonal anti-TIM23	This paper	#1526
Rabbit polyclonal anti-TIM21	This paper	#3674
Rabbit polyclonal anti-TOM20	Proteintech	Cat# 11802-1-AP; RRID: AB_2207530
Rabbit polyclonal anti-MITRAC12	This paper	#3761
Rabbit polyclonal anti-uL1m	This paper	#4964
Rabbit polyclonal anti-uL10m	Proteintech	Cat# 16652-1-AP; RRID: AB_2282109
Rabbit polyclonal anti-bL12m	Proteintech	Cat# 14795-1-AP; RRID: AB_2250805
Rabbit polyclonal anti-mL44	Proteintech	Cat# 16394-1-AP; RRID: AB_2146062
Rabbit polyclonal anti-mL45	Proteintech	Cat# 15682-1-AP; RRID: AB_2146065
Rabbit polyclonal anti-uS7m	Sigma-Aldrich	Cat# HPA023007; RRID: AB_1854132
Rabbit polyclonal anti-uS14m	Proteintech	Cat# 16301-1-AP; RRID: AB_2878240
Rabbit polyclonal anti-uS15m	Proteintech	Cat# 17006-1-AP; RRID: AB_2301068
Rabbit polyclonal anti-mS40	This paper	#5177
Goat anti-Rabbit Atto 647N	Rockland	Cat# 611-156-122; RRID: AB_10893043
Goat anti-Mouse STAR 580	Abberior	Cat# ST580-1001-500UG
Goat anti-Rabbit IgG (H+L) HRPO	Jackson ImmunoResearch	Cat# 111-035-144; RRID: AB_2307391
Goat anti-Mouse IgG (H+L) HRPO	Jackson ImmunoResearch	Cat# 115-035-166; RRID: AB_2338511
Bacterial and virus strains		
Escherichia coli BL21 Tuner (DE3)	Sigma-Aldrich	Cat# 70623
Chemicals, peptides, and recombinant proteins		
Sulfo DBCO-PEG4-Maleimide	Jena Bioscience	Cat# CLK-CSTM
DyLight 488 Maleimide	Thermo Scientific	Cat# 46602
Digitonin	Merck Millipore	Cat# 300410
[^{35}S] methionine	Hartmann Analytic	Cat# SCM-01
Lipofectamine RNAiMAX	Invitrogen	Cat# 13778075
GeneJuice	Sigma-Aldrich	Cat# 70967
X-tremeGENE 9 DNA transfection reagent	Roche	Cat# XTG9-RO

(*Continued on next page*)

Continued

REAGENT or RESOURCE	SOURCE	IDENTIFIER
Critical commercial assays		
nCounter XT TagSet24	nanoString	N/A
KOD Hot Start DNA Polymerase	Merck	Cat# 71086-3
mMessage mMachine SP6 transcription kit	Invitrogen	Cat# AM1340
Flexi Rabbit Reticulocyte Lysate System	Promega	Cat# L4540
Experimental models: Cell lines		
HEK293-Flp-In T-Rex (HEK293T)	ThermoFisher Scientific	RRID: CVCL_U421
HEK293T-uL1m^{FLAG}	This paper	N/A
HEK293T-mL45^{FLAG}	This paper	N/A
HEK293T-DHX30^{FLAG}	This paper	N/A
U2OS	ECACC General Collection	Cat# 92022711; RRID: CVCL_0042
Experimental models: Organisms/strains		
YPH499 MATa *ade2-101, his3-Δ200, leu2-Δ1, ura3-52, trp1-Δ63, lys2-801*	(Sikorski and Hieter, 1989)	Yeast collection #13
Oligonucleotides		
IGF2BP1 siRNA: UGGUACAGUAGAGAACUGU	Eurogentec	N/A
DHX30 siRNA: CACACGCCAUGUAUAACCU	Eurogentec	N/A
Probes A and B for mtRNA detection with TagSet	IDT	N/A
Morpholino oligonucleotides	Gene-Tools	N/A
Recombinant DNA		
pHis-SUMO-Jac1(C145A)-FLAG-Cys	This study	Plasmid #: R776
pHis-SUMO-Jac1(C145A)-Cys	This study	Plasmid #: R1015
pcDNA3.1_IGF2BP1	This study/ Genscript	N/A
pcDNA5-uL1m^{FLAG}	This study	N/A
pcDNA5-mL45^{FLAG}	This study	N/A
pcDNA5-DHX30^{FLAG}	This study	N/A
Software and algorithms		
ImageQuantTL v8.1	GE Healthcare	https://www.cytivalifesciences.com/en/us/shop/protein-analysis/molecular-imaging-for-proteins/imaging-software/imagequant-tl-8-1-p-00110
ImageJ v1.47	NIH	https://imagej.nih.gov/ij/download.html
Prism 8	GraphPad Software	https://www.graphpad.com/scientific-software/prism/
Perseus	(Tyanova et al., 2016)	N/A
nSolver	nanoString	https://www.nanostring.com/products/analysis-solutions/ncounter-analysis-solutions/
Other		
anti-FLAG M2 Affinity Gel	Sigma-Aldrich	Cat# A2220; RRID: AB_10063035

RESOURCE AVAILABILITY

Lead contact

Further information and requests for resources should be addressed to and will be fulfilled by the lead contact, Peter Rehling (peter.rehling@medizin.uni-goettingen.de).

Materials availability

Plasmids, cell lines, and other resources are available upon request to the lead contact.

Data and code availability

- All data reported in this paper will be shared by the lead contact upon request.

- This paper does not report original code.
- Any additional information required to reanalyze the data reported in this paper is available from the lead contact upon request.

EXPERIMENTAL MODEL AND SUBJECT DETAILS

Human-derived cell lines culture

HEK293T and U2OS cells were cultured in DMEM, supplemented with 10% (v/v) fetal bovine serum (Biochrom), 2 mM L-glutamine, 1 mM sodium pyruvate, and 50 μg/mL uridine, and incubated at 37°C with 5% CO_2.

For SILAC experiments, HEK293T cells were cultured in SILAC DMEM High Glucose lacking arginine and lysine (anprotec), supplemented with 10% (v/v) dialyzed fetal bovine serum (anprotec), 2 mM L-glutamine, 1 mM sodium pyruvate, 50 μg/mL uridine, Pen/Strep, and 200 mg/L proline. To prepare "light" medium (L), it was supplemented with 140 mg/L lysine and 100 mg/mL arginine (SERVA). The "heavy" medium (H) contained 140 mg/L lysine ($^{13}C_6$, $^{15}N_2$), and 100 mg/mL arginine ($^{13}C_6$, $^{15}N_4$) (Cambridge Isotope Laboratories). The cells were incubated at 37°C with 5% CO_2.

Bacterial culture

Escherichia coli BL21 Tuner (DE3) strain (Sigma-Aldrich) was used in this study. Cells were grown in LB medium (1% tryptone, 0,5% yeast extract, 10 g/L) supplemented with 2% glucose and 50 μg/mL kanamycin at 30°C in precultures. For recombinant protein expression, Cells were grown in LB medium supplemented with 50 μg/mL kanamycin at 30°C. After reaching the exponential growth phase, IPTG was added and the culture shifted to 25°C.

Yeast culture

Saccharomyces cerevisiae YPH499 cells (Sikorski and Hieter, 1989) were grown at 30°C in YP media (1% yeast extract, 2% peptone) containing 3% glycerol (YPG), as carbon source.

METHOD DETAILS

Recombinant Jac1 expression and purification

Recombinant proteins Jac1 containing a FLAG tag or a mutated FLAG tag were purified as follows. Plasmids derived from the K27 plasmid (Gomkale et al., 2021), containing a His_{14}-SUMO-tag fused at the N terminus of Jac1(C145A) and a cysteine group at the C terminus, were transformed in the *Escherichia coli* BL21 Tuner (DE3) strain (Sigma-Aldrich). One colony was inoculated into 5 mL LB medium supplemented with 2% glucose and 50 μg/mL kanamycin. The preculture was incubated for eight h at 30°C. The OD_{600nm} was determined. 100 mL of fresh medium was inoculated at initial OD_{600nm} = 0.1 and incubated overnight at 30°C. Next, the preculture was diluted in 2L of LB medium supplemented with 50 μg/mL kanamycin to OD_{600nm} = 0.05. The culture was incubated at 30°C until the OD_{600nm} reached 0.6-0.8. Then, protein expression was induced with 0.2 mM IPTG, the culture transferred to 25°C, and incubated for additional five h. The cells were harvested and kept at −80°C for further experiments.

Harvested cells were resuspended in lysis buffer (40 mM Tris/HCl, 500 mM NaCl, 10 mM Imidazole, 1mM PMSF, 0.2 mg/mL DNase1, 1x complete protease inhibitor cocktail, pH 7.4). Cell disruption was performed with an EmulsiFlex-C3 (AVESTIN). The lysate was cleared by centrifugation in an SS-34 rotor at 23000xg 4°C for 60 min. Next, the supernatant was collected and injected in a HisTrap 1ml column (Cytiva) pre-equilibrated in buffer A1 (40 mM Tris/HCl, 500 mM NaCl, 10 mM Imidazole, pH 7.4). After exhaustive washing with buffer A2 (40 mM Tris/HCl, 500 mM NaCl, 30 mM Imidazole, pH 7.4), the bound protein was eluted in a gradient 0%–100% of buffer B (40 mM Tris/HCl, 500 mM NaCl, 500 mM Imidazole, pH 7.4). The SUMO-Jac1 containing fractions were pooled, and the buffer was exchanged to 20 mM Tris/HCl, 150 mM NaCl, pH 7.4 in HiPrep 26/10 Desalting column (Cytiva). The protein was digested with His_6-SUMO protease overnight at 4°C in the presence of 5mM DTT. Then, to the digestion mix was added one volume of buffer C (60 mM Tris/HCl, 850 mM NaCl, 100 mM Imidazole, pH 7.4) and two volumes of buffer A. The mix was injected into a HisTrap 1ml column (Cytiva) to remove non-cleaved protein, His-SUMO tag, and His-SUMO protease. The unbound fraction was collected, concentrated, and the buffer was exchanged to 20 mM Tris/HCl, 150 mM NaCl, 5% glycerol, pH 7.4 in HiPrep 26/10 Desalting column (Cytiva).

Synthesis of $Jac1_{488}$, Jac1-DBCO, and Jac1-oligonucleotide chimera

To guarantee the reduction of the thiol group in Jac1, TCEP (Sigma-Aldrich) was added to the purified Jac1 to a final concentration of 5 mM. The mix was incubated for two h at RT. The excess of TCEP removed by buffer exchange to Maleimide buffer (100 mM potassium phosphate, 150 mM NaCl, 250 mM sucrose, 1mM EDTA, pH 6.6) in HiPrep 26/10 Desalting column (Cytiva).

To fluorescently label Jac1, 50 μM DyLight488-maleimide was added to the reduced protein and incubated overnight at 4°C with end-to-end mixing. Next, the excess of maleimide groups was quenched with a 50-fold molar excess of cysteine versus the maleimide concentration. Finally, the buffer was exchanged to 20 mM Tris/HCl, 150 mM NaCl, 5% glycerol, pH 7.4 in PD10 desalting columns (Cytiva). The protein concentration was determined and set to 1 mg/mL. Aliquots of the labeled protein ($Jac1_{488}$) were kept at −80°C until used.

For the synthesis of Jac1-DBCO, sulfo-DBCO-PEG_4-maleimide (Jena Bioscience) was added to the reduced Jac1 in 20-fold molar excess. The mix was incubated overnight at 4°C with end-to-end mixing. Next, the excess of maleimide groups was quenched with a 50-fold molar excess of cysteine versus the maleimide concentration. Finally, the buffer was exchanged to 20 mM Tris/HCl, 150 mM NaCl, 5% glycerol, pH 7.4 in HiPrep 26/10 Desalting column (Cytiva). The protein concentration was determined and set to 1 mg/mL. Aliquots of the DBCO-modified protein (Jac1-DBCO) were kept at −80°C until use.

Jac1-oligonucleotide chimeras were synthesized by mixing Jac1-DBCO with an 8-fold molar excess of single-stranded DNA (ssDNA) and RNA oligonucleotides (Microsynth), and morpholino phosphorodiamidate oligonucleotides (MO) (Gene Tools) containing 5′-[azide] and 3′-[FITC] groups. The click reaction was carried out at 25°C for two h.

Cell culture

HEK293-Flp-In T-Rex (HEK293T), HEK293T-derived, and U2OS cells were cultured in DMEM, supplemented with 10% (v/v) fetal bovine serum (Biochrom), 2 mM L-glutamine, 1 mM sodium pyruvate, and 50 μg/mL uridine, and incubated at 37°C with 5% CO_2.

For SILAC experiments, HEK293T cells were cultured in SILAC DMEM High Glucose lacking arginine and lysine (anprotec), supplemented with 10% (v/v) dialyzed fetal bovine serum (anprotec), 2 mM L-glutamine, 1 mM sodium pyruvate, 50 μg/mL uridine, Pen/Strep, and 200 mg/L proline. To prepare ''light'' medium (L), it was supplemented with 140 mg/L lysine and 100 mg/mL arginine (SERVA). The ''heavy'' medium (H) contained 140 mg/L lysine ($^{13}C_6$, $^{15}N_2$), and 100 mg/mL arginine ($^{13}C_6$, $^{15}N_4$) (Cambridge Isotope Laboratories). The cells were incubated at 37°C with 5% CO_2.

HEK293T-uL1m^{FLAG} and HEK293T-mL45^{FLAG} cell lines were generated as described recently (Richter-Dennerlein et al., 2016). The open reading frame of uL1m (NM_020236.3) and mL45 (NM_032351.5) were cloned into pcDNA5/FRT/TO with the sequence corresponding to a C-terminal FLAG tag. HEK293T cells were transfected with pOG44 and pcDNA5-uL1m^{FLAG} or pcDNA5-uL1m^{FLAG} using GeneJuice. Cells were selected with 100 μg/mL hygromycin for approximately two weeks and single clones were tested for expression by western blotting and immunodetection.

Moreover, HEK293T-DHX30^{FLAG} cells were generated as follows. The coding sequence of DHX30 (NM138615) was cloned into a pcDNA5-based plasmid for the expression of C-terminally His_6-PreScission protease cleavage site-2xFLAG (FLAG) tagged DHX30 in human cells. HEK293T cells were transfected with pcDNA5-DHX30^{FLAG} using X-tremeGENE 9 DNA transfection reagent (Roche) according to the manufacturer's instructions. Stably transfected cells were selected using 100 ug/mL hygromycin and 10 ug/mL blasticidin.

HEK293T cells with C-terminal FLAG-tagged C12ORF62 (C12ORF62^{FLAG}) (Richter-Dennerlein et al., 2016), uL1m (uL1m^{FLAG}), and mL45 (mL45^{FLAG}) genome-integrated were cultured in the conditions described above. Expression of the FLAG-tagged proteins was induced with 0.6 μg/mL tetracycline for 24 h.

HEK293T cell expressing DHX30^{FLAG} were cultured as described previously (Haag et al., 2016) and expression of the fusion protein was induced with 1 μg/mL tetracycline for 24 h.

In vivo [^{35}S] methionine labeling of mitochondrial translation products

The medium of HEK293T cells was exchanged to DMEM without methionine. The cytosolic translation was inhibited with 100 μg/mL emetine for 10 min. Next, 200 μCi/mL of [^{35}S] methionine were added, and the cells were incubated for one h at 37°C with 5% CO_2. The cells were harvested, and equivalent protein amounts were mixed with SDS-PAGE loading dye buffer for the analysis in Tris-Tricine 10%–18% gradient gels. After transferring the proteins to a PVDF membrane, the radioactive signal was detected by digital autoradiography.

siRNA-mediated protein knockdown

siRNA targeting IGF2BP1 and DHX30 mRNA and a non-targeting siRNA (siNT) were purchased from Eurogentec (Liege, Belgium). HEK293T cells (1x10^6 cells) were transfected with Lipofectamine RNAiMAX (Invitrogen) following the manufacturer's instructions and transferred to a T25 cell culture flask. Cells were transfected for 72 h and then used for further analyses. DHX30 siRNA was used at 50 nM final concentration in all experiments. IGF2BP1 siRNA was used at 50 nM final concentration in all experiments except for *in vivo* [^{35}S] methionine labeling of mitochondrial translation products, where 33 nM was used.

IGF2BP1^{FLAG} transient expression in HEK293T

The IGF2BP1 ORF inserted in pcDNA3.1 plasmid, in frame with a C-terminal FLAG tag, was purchased from Genscript (Leiden, the Netherlands).

For immunofluorescence microscopy, pcDNA3.1-IGF2BP1 was transfected in U2OS cells using GeneJuice according to the manufacturer's instructions. The cells were then incubated for two days, being IGF2BP1^{FLAG} constitutively expressed.

For FLAG immunoisolation experiments, pcDNA3.1-IGF2BP1 was transfected using PEI (polyethylenimin) transfection reagent. Briefly, HEK293T cells were seeded to a confluency of 50% two days prior transfection. 100 μL PEI (stock 10mg/mL) were mixed with 400 μL OptiMEM and incubated at RT for 5minutes, prior adding 4.5 mL OptiMEM. For the transfection, 1 mL PEI/OptiMEM mix was transferred to a new tube containing 25 μg plasmid DNA and 1 mL OptiMEM. After a 20 min incubation at RT, 10 mL standard DMEM media was added and the mixture carefully transferred to a 15 cm cell culture dish. After incubation under standard growth condition for 3 h, 20 mL DMEM was added and transfected cells for 24 h cultured prior harvest.

Isolation of mitochondria from HEK293T cells

Mitochondria were isolated as previously described (Gomkale et al., 2020). Briefly, cells were washed with ice-cold isotonic buffer (10 mM MOPS pH 7.2, 225 mM sucrose, 75 mM mannitol, and 1 mM EGTA). Then, the cell pellet weight was determined. The pellet was resuspended in 5mL/(g cells) of cold hypotonic buffer (10 mM MOPS pH 7.2, 100 mM sucrose, and 1 mM EGTA) supplemented with 2 mM PMSF and incubated on ice for 6 min. The cell suspension was homogenized in a Dounce glass homogenizer. Cold hypertonic buffer (1.25 M sucrose and 10 mM MOPS pH 7.2) was added to the cell homogenate 1.1 mL/(g cells), and the volume doubled with isotonic buffer supplemented with 2 mM PMSF and 2 mg/mL BSA. The homogenate was subjected to centrifugation at 1000 x g for 10 min at 4°C, the supernatant recovered, and the same step repeated. Mitochondria were pelleted by centrifuging the supernatant at 11000 xg for 10 min at 4°C and washed once with isotonic buffer without BSA. Finally, the pellet was resuspended in isotonic buffer, and the protein concentration of isolated mitochondria was determined using the Bradford assay.

Isolation of mitochondria from *Saccharomyces cerevisiae* cells

YPH499 cells (Sikorski and Hieter, 1989) were grown at 30°C in YP media (1% yeast extract, 2% peptone) containing 3% glycerol (YPG), as carbon source, to OD_{600} of 1.5-2.5 and then harvested. The pellet was washed with water and then treated in DTT buffer (10 mM DTT, 100 mM Tris/H_2SO_4, pH 9.4) for 30 min at 30°C with shaking. Subsequently, cells were washed and treated with Zymolyase buffer (20 mM KPO_4, pH 7.4, 1.2 M sorbitol, and 0.57 mg/L zymolyase) for 1 h with shaking at 30°C. Cells were sedimented and washed with zymolyase buffer. The cells were resuspended in cold homogenization buffer (600 mM sorbitol, 10 mM Tris/HCl, pH 7.4, 1 g/L BSA, 1 mM PMSF, and 1 mM EDTA), and then homogenized using a glass/teflon Potter-Elvehjem homogenizer. Mitochondria were obtained by differential centrifugation and resuspended in SEM buffer (250 mM sucrose, 20 mM MOPS/KOH pH 7.2, 1 mM EDTA). They were aliquoted in appropriate volume, flash frozen in liquid nitrogen, and stored at −80°C.

Import of $Jac1_{488}$ into HEK293T mitochondria

Freshly isolated mitochondria were resuspended at 1 mg/mL in import buffer (20 mM HEPES, 100mM mannitol, 80 mM KCl, 5 mM $MgCl_2$, 10 mM sodium succinate, 10 mM malate, 5 mM ATP, 6 mM creatine phosphate, 0.625 mg/mL creatine kinase, 1 mg/mL BSA, 5 mM NADH, pH 7.4). The mitochondrial suspension was distributed in 50 μL aliquots, and the import reaction started by adding 5 μL of $Jac1_{488}$. The samples were incubated at 37°C under mild shaking conditions for different periods. The reaction was stopped by adding AVO mix (final concentration 1 μM valinomycin, 8 μM antimycin A, and 20 μM oligomycin) to disrupt the membrane potential. Samples were treated with 20 μg/mL Proteinase K (PK) for 10 min on ice. PK was inactivated with 2 mM phenylmethylsulphonyl fluoride (PMSF) for 10 min on ice. The mitochondria were sedimented at 11000xg, washed once with isotonic buffer, and the proteins resolved by SDS-PAGE. Finally, the gel was scanned in a Starion FLA-9000 (FUJIFILM) using the appropriate settings.

Jac1-FLAG protein was used for most of the experiments, except for the experiment with mitochondria isolated from FLAG-tagged protein-expressing cells, when the mutated FLAG variant was used.

Import of [^{35}S]Jac1 into *Saccharomyces cerevisiae* and HEK293T mitochondria

Jac1(C41A)-FLAG-Cys DNA sequence was amplified by PCR, adding a SP6 polymerase-binding site at the 5′ end. In parallel, SP6-binding sequence was added to a truncated Jac1 without presequence, by removing the first ten amino acids. mMessagemMachine SP6 transcription kit (Invitrogen) was used to generate mRNAs *in vitro*, from both recombinant fragments, based on the manufacturer's instructions. For synthesis of [^{35}S] methionine labeled protein, *in vitro* translation was carried out using the Flexi Rabbit Reticulocyte Lysate System (Promega), obtaining [^{35}S]Jac1(C41A)-FLAG-Cys ([^{35}S]Jac1) and [^{35}S]ΔMTS-Jac1(C41A)-FLAG-Cys ([^{35}S]ΔMTS-Jac1) . The truncated version was used as an indicator for the processed form of [^{35}S]Jac1.

Import reactions of [^{35}S]Jac1 in yeast mitochondria were performed as previously described (Gomkale et al., 2020). Briefly, mitochondria were suspended in import buffer (250 mM sucrose, 10 mM MOPS/KOH pH 7.2, 80 mM KCl, 2 mM KH_2PO_4, 5 mM $MgCl_2$, 5 mM methionine and 3% fatty acid-free BSA) supplemented with 2 mM ATP, 2 mM NADH, 5 mM creatine phosphate and 0.1 mg/mL creatine kinase. Import was performed at 25°C for different time points and terminated using AVO mix to disrupt the membrane potential. Samples were treated with 20 μg/mL Proteinase K (PK) for 10 min on ice. PK was inactivated with 2 mM phenylmethylsulphonyl fluoride (PMSF) for 10 min on ice. Mitochondria were subsequently sedimented and washed with SEM buffer.

The import of [^{35}S]Jac1 in HEK293T mitochondria was perfomed as described in the previous section.

Import of Jac1-oligonucleotide chimera into human mitochondria

Freshly isolated mitochondria were resuspended at 1 mg/mL in import buffer (20 mM HEPES, 100 mM mannitol, 80 mM KCl, 5 mM $MgCl_2$, 10 mM sodium succinate, 10 mM malate, 5 mM ATP, 6 mM creatine phosphate, 0.625 mg/mL creatine kinase, 1 mg/mL BSA, 5 mM NADH, pH 7.4). The mitochondrial suspension was distributed in 100 μL aliquots, and the import reaction was started by adding 2 μM Jac1-oligonucleotide hybrids as the final concentration. The samples were incubated at 37°C under mild shaking conditions for 30 min. The reaction was stopped by adding AVO mix (final concentration 1 μM valinomycin, 8 μM antimycin A, and 20 μM oligomycin) to disrupt the membrane potential. Samples were treated (+PK) or not (-PK) with 20 μg/mL PK for 10 min on ice. PK was inactivated with 2 mM phenylmethylsulphonyl fluoride (PMSF) for 10 min on ice. The mitochondria were sedimented at 11000xg for 10 min, washed once with isotonic buffer, and the proteins resolved in 4%–12% NuPAGE Bis-Tris (Invitrogen). Finally, the gel was scanned in a Starion FLA-9000 (FUJIFILM) with the appropriate settings.

Downregulation of mtDNA-encoded genes by Jac1-morpholino chimera in human mitochondria

For the downregulation of mtDNA-encoded genes, Jac1-MO hybrids were imported as described above for 30 min, unless otherwise indicated. Briefly, freshly isolated mitochondria were resuspended at 1 mg/mL in import buffer (20 mM HEPES, 100mM mannitol, 80 mM KCl, 5 mM $MgCl_2$, 10 mM sodium succinate, 10 mM malate, 5 mM ATP, 6 mM creatine phosphate, 0.625 mg/mL creatine kinase, 1 mg/mL BSA, 5 mM NADH, pH 7.4). As a negative control for the import, AVO mix was added before. The import reaction was started by adding 2 μM Jac1-MO hybrids as the final concentration or an equivalent amount of free MO when required. The samples were incubated at 37°C under mild shaking conditions for 30 min unless otherwise indicated. To stop the reaction, the samples were placed on ice. Then, the mitochondria were sedimented 11000xg for 10 min. Next, the mitochondria were resuspended in import buffer (25 mM HEPES, 100mM mannitol, 80 mM KCl, 5 mM $MgCl_2$, 10 mM sodium succinate, 1 mM potassium phosphate, 5 mM ATP, 6 mM creatine phosphate, 0.625 mg/mL creatine kinase, 1 mg/mL BSA, 0.02 mM GTP, 0.15mM amino acid mix (minus methionine), 100 μg/mL emetine, pH 7.4) (modified from Côté et al., 1989). The negative control for the translation reaction was obtained by adding 0.3 mg/mL chloramphenicol. Samples were incubated for 5 min at 37°C, 100 μCi/mL of [^{35}S] methionine were added, and the translation was performed for one h at 37°C. When required, the translation was stopped by adding 0.3 mg/mL chloramphenicol. Finally, mitochondria were sedimented and used for follow-up experiments or analysis.

In the case of experiments where the imported chimera quantities had to be checked, mitochondria were treated with PK as described above, and the import efficiency assessed by quantification of the FITC-detected fluorescence as intensity ratio to a known amount of synthesized Jac1-MO after Tris-Tricine 10%–18% gradient gel analysis.

Titrating the effect of imported Jac1-COX1$^{1-19}$ on mitochondrial translation

To assess the correlation between the quantity of imported Jac1-COX1$^{1-19}$ and the degree of COX1 synthesis downregulation, HEK293T mitochondria were incubated in the presence of different Jac1-COX1$^{1-19}$ concentrations for 30 min. Then, samples were subjected to translation and proteinase K treatment, and analyzed by SDS-PAGE. A known amount of synthesized Jac1-COX1$^{1-19}$ was loaded in the same gel. the gel was scanned in a Starion FLA-9000 (FUJIFILM) with the appropriate settings. The fluorescence intensity corresponding to the FITC in Jac1-COX1$^{1-19}$ was quantified for each condition, and the molar amount estimated based on the reference.

Blocking the presequnce import pathway with Jac1-sfGFP prior Jac1-COX1$^{1-19}$ import

To corroborate the Jac1-COX1$^{1-19}$ import dependence on the presequence import pathway, Jac1-sfGFP was used as a blocking agent (Gomkale et al., 2021). HEK293T mitochondria were incubated in the presence of different concentrations of Jac1-sfGFP for 30 min at 37°C. The mitochondria were sedimented, resuspended in fresh import buffer, and 2 μM of Jac1-COX1$^{1-19}$ was added to start the import reaction. The samples were incubated for 10 min at 37°C, and processed for downregulation experiments. The fluorescence intensity corresponding to the FITC in Jac1-COX1$^{1-19}$ was quantified for each condition, and the molar amount estimated based on a reference amount loaded in the same gel.

Downregulation of mtDNA-encoded genes by Jac1-morpholino chimera in mouse brain mitochondria

Mice were maintained and studied according to the guidelines from the German Animal Welfare Act and approved by the Landesamt fuer Verbraucherschutz und Lebensmittelsicherheit, Niedersachsen, Germany (AZ: 33.9-42502-04-15/1991). WT C57BL/6N were euthanized with exposure to anesthesia and subsequent cervical dislocation for tissue harvest. Brains were homogenized using motorized Teflon potters, and mitochondria were isolated by differential centrifugation according to the standard liver mitochondria protocol (Frezza et al., 2007). Following mitochondrial isolation, Bradford estimation for total protein amounts was performed.

The import of Jac1-MO hybrids was performed for 30 min as described above for human mitochondria.

Post-import, the mitochondria were washed by centrifugation and resuspended in translation buffer for *in vitro* translation assay. Standard reaction conditions were as follows, unless otherwise indicated: 2 mg/mL mitochondria, 25 mM sucrose, 100 mM Mannitol, 80 mM KCl, 5 mM $MgCl_2$, 1 mM Kpi pH 7.4, 25 mM HEPES-KOH pH 7.4, 6mM ATP, 0.75 mM GTP, 12 mM Creatine phosphate, 10 mM sodium succinate, 0.625 mg/mL creatine kinase, 9 mM 2-ketoglutarate, 0.15 mM amino acid mix, 100 μg/mL emetine, 100 μg/mL cycloheximide, 2.5 mM malate, 1 mg/mL BSA and 1X protease inhibitor cocktail. Incubations with 100μCi/mL of [^{35}S] methionine were carried out for one h at 37°C unless otherwise indicated. Translations were stopped by the addition of 0.3 mg/mL chloramphenicol, washed, and processed for Tris-Tricine SDS-PAGE analysis.

Native immunoprecipitation of FLAG-tagged proteins

Protein complex isolation by FLAG immunoisolation was performed as previously described (Richter-Dennerlein et al., 2016). Briefly, cells or mitochondria were solubilized at 1 mg/mL protein concentration in lysis buffer (50 mM Tris/HCl pH 7.4, 150 mM NaCl, 10% glycerol, 10 mM $MgCl_2$, 1% Digitonin, 1 mM PMSF, 1x complete protease inhibitor cocktail, 0.08 U/μL RiboLock RNase inhibitor) for 30 min on ice with periodic mixing. The insoluble material was removed by centrifugation at 10000 xg for 10min at 4°C. The lysate was then mixed with anti-FLAG M2 Affinity Gel (Sigma-Aldrich) and incubated for one h at 4°C. Next, the unbound fraction was removed and the resin washed with washing buffer (50 mM Tris/HCl pH 7.4, 150 mM NaCl, 10% glycerol, 10 mM $MgCl_2$, 0,1% Digitonin, 1 mM PMSF, 1x complete protease inhibitor cocktail, 0.08 U/μL RiboLock RNase inhibitor). The native protein complexes were eluted with

FLAG peptide in washing buffer for 30 min at 4°C. HEK293T cells or derived mitochondria were used as negative controls. Equivalent amounts of material were analyzed by SDS-PAGE and western blotting.

Protease protection assay

For protein submitochondrial localization, HEK293T isolated mitochondria were resuspended either in SEM buffer (250 mM sucrose,1 mM EDTA, and 10 mM MOPS pH 7.2) or, to permebalize the outer mitochondrial membrane, in hypoosmotic swelling buffer (EM buffer) (1 mM EDTA, and 10 mM MOPS pH 7.2). Proteinase K (PK) was added (final concentration 50 or 100 μg/mL) and samples incubated on ice for 25 min. As controls, mitochondria were lysed by sonication or by addition of Triton X-100 (final 1%) in the presence of PK. PK was inhibited in all samples by adding PMSF (2 mM final concentration) and further incubation on ice for 10 min. The samples were resolved under denaturing conditions on 10%–18% Tris-Tricin gels, and analyzed by western blotting.

Mitochondrial RNA detection by nanoString technology

Immunoisolation input and eluate fractions were mixed with Trizol reagent (Thermo Scientific Fisher), and the RNA purified using RNA Clean & Concentrator kit (Zymo Research) following the manufacturer's instructions.

For the analysis of siRNA-treated cells, mitochondria were isolated and solubilized in lysis buffer with 1% digitonin as it was described above. The cleared lysate was then processed for RNA isolation.

Equivalent amounts of RNA were mixed with a TagSet-24 and detection primers (IDT) previously used to detect mitochondrial transcripts (Richter-Dennerlein et al., 2016). Next, the samples were processed and analyzed in a nCounter MAX analysis system (nanoString) following the manufacturer's instructions. The acquired data were analyzed with nSolver software (nanoString).

Protein electrophoresis and immunodetection

The recombinant protein purification, modification process, and protein-morpholino synthesis were followed by SDS-PAGE in 4%–12% NuPAGE Bis-Tris (Invitrogen). Experiments of $Jac1_{488}$ and Jac1-(ssDNA/RNA/MO) import were analyzed by SDS-PAGE in 4%–12% NuPAGE Bis-Tris (Invitrogen).

Tris-Tricine 10%–18% gradient gel electrophoresis was used to analyze the samples obtained in downregulation of mitochondrial translation experiments and samples from immunoisolation experiments.

Native complexes solubilized in solubilization buffer (20 mM Tris/HCl pH 7.4, 150 mM NaCl, 10% glycerol, 1 mM EDTA, 1 mM PMSF, 1x complete protease inhibitor cocktail) containing 1% digitonin (for further second dimension SDS) or 0.3% DDM (for immunodecoration) were resolved by 4%–13% Blue Native (BN)-PAGE. When required, the lanes were excised, assembled in a Tris-Tricine 10%–18% gradient gel, and resolved in a second dimension (2D).

After the electrophoresis, the proteins were often transferred to PVDF membranes, then exposed to a phosphoscreen for digital autoradiography with Typhoon imaging system (GE Healthcare) or processed for western blotting.

Northern blot

Total RNA was isolated from whole-cell extracts using Trizol reagent, separated by agarose gel electrophoresis under denaturing conditions (5.5% formaldehyde, 35% formamide), and blotted to Amersham Hybond^{TM}-N membrane (GE Healthcare). After UV-crosslinking, the membranes were incubated with [^{32}P]-radiolabelled probes overnight. Probes were generated to target the specific mitochondrial RNAs, and the radioactive label was incorporated using T4 polynucleotide kinase (ThermoScientific) according to the manufacturer's instructions. The resulting signals were visualized with a Typhoon imaging system (GE Healthcare).

Mitochondria isolation and sucrose density gradient ultracentrifugation

Mitochondria were isolated from cultured cells as described in Lavdovskaia et al., 2018. Briefly, cells were homogenized in trehalose buffer (300 mM trehalose, 10 mM KCl, 10 mM HEPES-KOH pH 7.4, 1 mM PMSF, and 2 mg/mL BSA) using Homogen^{plus} Homogenizer (Schuett-Biotec). Mitochondria (250 μg) were lysed in lysis buffer (3% sucrose, 100 mM KCl, 15 mM $MgCl_2$, 20 mM HEPES-KOH, pH 7.4, 1% digitonin, 1x complete protease inhibitor cocktail, and 0.08 U/μl RiboLock RNase Inhibitor) and loaded on a 5%–30% sucrose (w/v) sucrose gradient. Ribosomal particles were separated at 79,000xg, 4°C for 15 h using SW41 Ti (Beckman Coulter). Fractions (1-16) were collected with BioComp fractionator and analyzed by western blotting.

LC-MS/MS analysis

Proteins were denatured by 1% SDS and subsequently reduced and alkylated by 5 mM TCEP and 20 mM CAA, respectively. Samples were cleaned up following the SP3 protocol (Moggridge et al., 2018). Proteins were digested with trypsin in a 1:50 enzyme-to-protein ratio in 50 mM ammonia bicarbonate on beads overnight. Eluted peptides were desalted using MicroSpin columns following the manufacturer's instructions. Desalted peptides were vacuum-dried and subsequently resuspended in 2% acetonitrile (ACN, v/v)/0.05% trifluoroacetic acid (TFA, v/v). Peptides were measured on a QExactive HF Mass Spectrometer coupled to a Dionex UltiMate 3000 UHPLC system (both Thermo Fisher Scientific) equipped with an in-house-packed C18 column (ReproSil-Pur 120 C18-AQ, 1.9 μm pore size, 75 μm inner diameter, 30 cm length, Dr. Maisch GmbH). Peptides were separated applying the following gradient: mobile phase A consisted of 0.1% formic acid (FA, v/v), mobile phase B of 80% ACN/0.08% FA (v/v). The gradient started at 5% B,

increasing to 10% B within 3 min, followed by a continuous increase to 46% B within 74 min, and then keeping B constant at 90% for 5 min. After each gradient, the column was again equilibrated to 5% B. The flow rate was set to 300 nL/min. MS1 full scans were acquired with a resolution of 60,000, an injection time (IT) of 50 ms, and an automatic gain control (AGC) target of 1 × 106. Dynamic exclusion (DE) was set to 45 s. MS2 spectra were acquired of the 30 most abundant precursor ions; the resolution was set to 15,000; the IT was set to 128 ms, and the AGC target to 1 × 105. Fragmentation was enforced by higher-energy collisional dissociation (HCD) at 30% NCE. Acquired raw data were analyzed by MaxQuant (v. 1.6.0.1) (Cox and Mann, 2008) applying default settings. Lys8/Arg10 were selected as heavy labels, and 'match between runs' option was enabled.

Volcano plot and heatmap preparation

Volcano plots were prepared using the Perseus software platform (Tyanova et al., 2016). Reversed ratios were transformed according to the formula $x^{(-1)}$. Subsequently, all values were $\log_2$-transformed. Three out of four valid values per protein were considered for further calculations. A one-sample t test was performed (s-value = 0, both sides, threshold p value = 0.05, corrected according to Benjamini-Hochberg) and the $-\log_{10}$-transformed corrected p value was plotted against the fold change.

Heatmaps were prepared using the R software platform (R Development Core Team, 2014) and its function heatmap.2. For this, $\log_2$-transformed fold changes were taken from the volcano plots and plotted for all three experiments. Here, only proteins of the mitochondrial ribosome were considered.

Immunostaining for confocal and STED microscopy

Standard protocols for immunostaining were applied. Briefly, cells on glass coverslips were fixed for 30 min with 4% Polyformaldehyde solution (PFA) and were quenched for 15 min in 100 mM NH_4Cl in PBS, permeabilized, and blocked in a staining solution containing 2% BSA (Sigma-Aldrich) supplemented with 0.1% Triton X-100 (Merck) in PBS. Primary antibodies were diluted at 1:200 in staining solution and applied for one h at room temperature. Three 5 min washing steps with the staining solution were performed, then the secondary antibodies were diluted 1:200 in the same solution and applied for one h. Following sequential washing steps with blocking solution (2% BSA in PBS) and PBS, the coverslips were embedded in Mowiol (Merck) and were dried overnight at room temperature before imaging.

For the immunodetection, $IGF2BP1^{FLAG}$ was detected with mouse monoclonal anti-FLAG (Sigma-Aldrich) and TOM20 with rabbit polyclonal anti-TOM20 (Proteintech) antibodies. Besides, anti-mouse Abberior STAR 580 and anti-Rabbit Atto 647N (Sigma-Aldrich) were used as secondary antibodies.

Image acquisition

Confocal images were taken at an Abberior microscope operated with Inspector imaging software (Abberior). This setup was built on an Olympus IX83 base, equipped with a UPlanSApo 100 × oil immersion objective (Olympus Corporation) and an EMCCD iXon Ultra camera (Andor). Pulsed 561-nm and 640-nm lasers were used for excitation of STAR580 and Atto647N, respectively. A 775 nm depletion laser was used to acquire high-resolution STED images. Where mentioned, images were deconvolved using Huygens software (Scientific Volume Imaging, https://svi.nl/).

QUANTIFICATION AND STATISTICAL ANALYSIS

Autoradiographic and western blot signal intensities were quantified with ImageQuantTL v8.1 (GE Healthcare) and ImageJ v1.47 (NIH).

Data were obtained from three or more biological replicates (n), and were processed with GraphPad Prism 8 software for statistical purposes. Mean, SEM, and statistical significance were used in the figure preparation as indicated in the figure legends.

CellPress
OPEN ACCESS

Supplemental figures

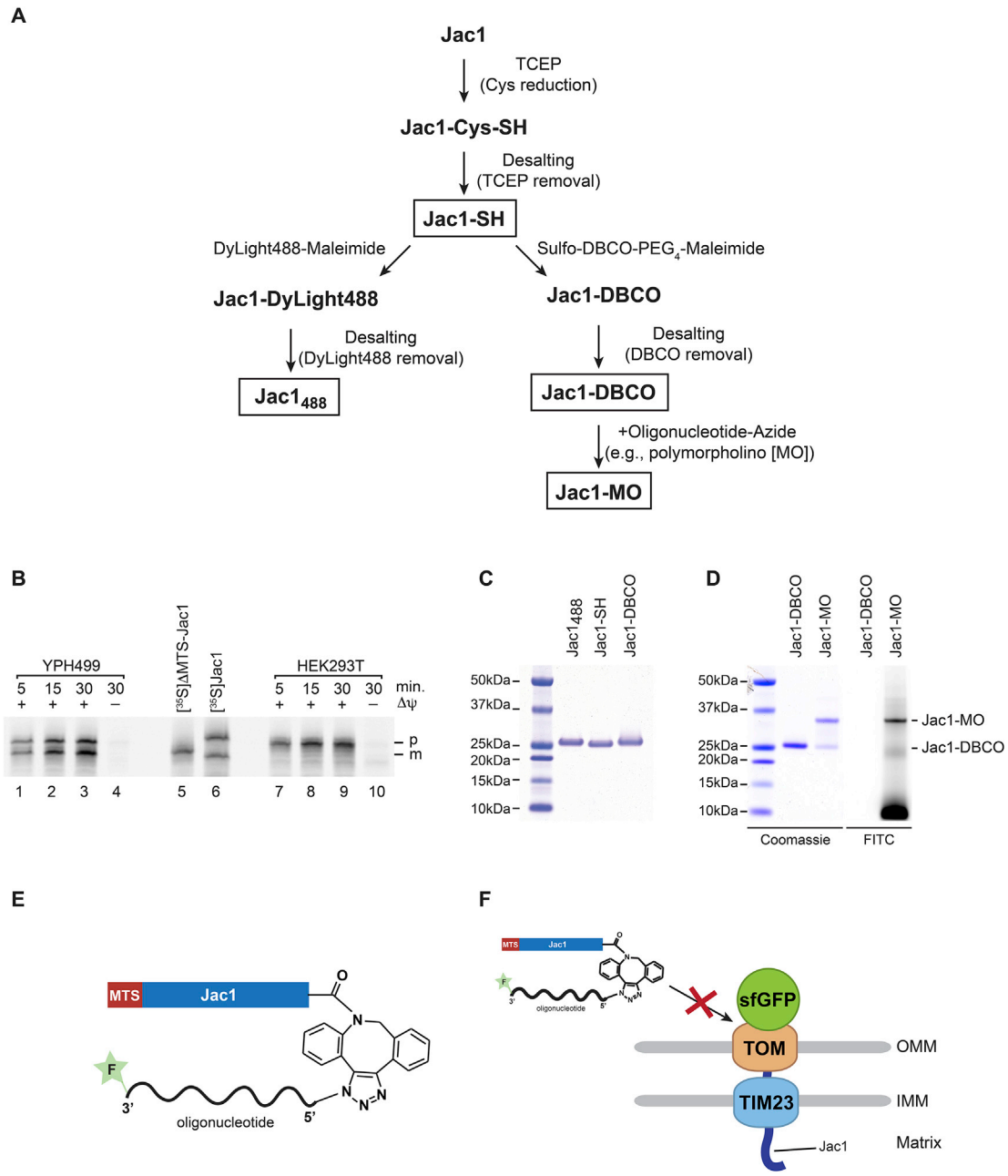

Figure S1. Synthesis and import of precursor-oligonucleotide hybrids, related to Figure 1

(A) Experimental workflow for the synthesis of $Jac1_{488}$, Jac1-DBCO, and Jac1-morpholino chimeras.

(B) [^{35}S]Jac1 was imported into mitochondria isolated from *Saccharomyces cerevisiae* or HEK293T cells, and treated with Proteinase K. The samples were analyzed by SDS-PAGE and digital autoradiography. [^{35}S]Jac1 with or without presequence (ΔMTS-Jac1) were used as reference. p, precursor; m, mature; Δψ, membrane potential.

(C) Coomassie-stained SDS-PAGE showing reduced Jac1 (Jac1-SH), Jac1 coupled to DyLight488, and DBCO to produce $Jac1_{488}$ and Jac1-DBCO, respectively.

(D) Example of click-reaction process for coupling Jac1-DBCO to oligonucleotides.

(E) Schematic presentation of the Jac1-oligonucleotide chimera. F, FITC group; MTS, mitochondrial targeting signal.

(F) Schematic presentation of translocase-associated Jac1-sfGFP blocking the presequence import pathway. OMM, outer mitochondrial membrane; IMM, inner mitochondrial membrane.

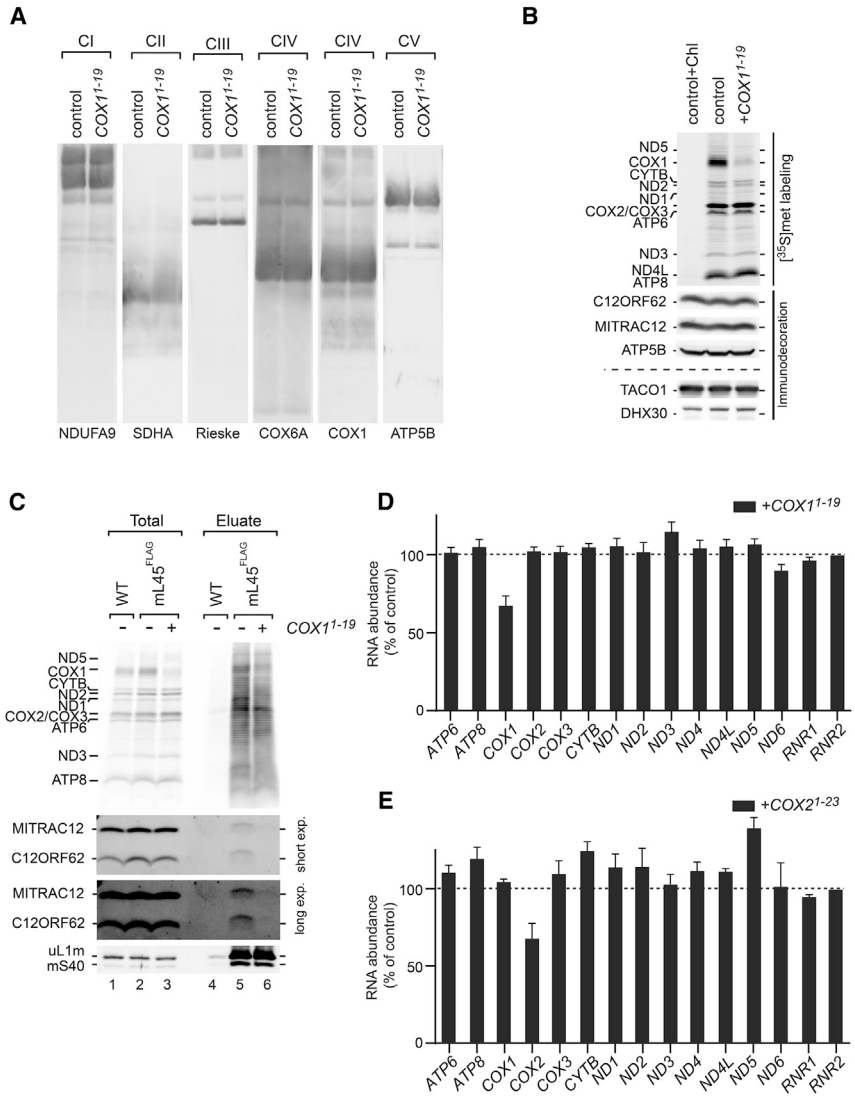

Figure S2. Effect of COX1 translation block on mitochondria protein levels, related to Figures 2 and 4

(A) Immunodetection of mitochondrial respiratory complexes by BN-PAGE after treatment of mitochondria with *COX1*$^{1-19}$. CI, complex I; CII, complex II; CIII, complex III; CIV, complex IV; CV, complex V.

(B) Steady-state levels of TACO1 and early complex IV assembly factors (C12ORF62 and MITRAC12) after blocking COX1 synthesis (assessed by radiolabeling of mitochondrial translation products, upper panel). ATP5B and DHX30 were used as loading controls.

(C) Mitochondrial ribosomes were isolated from HEK293T mL45m^{FLAG} purified mitochondria via FLAG immunoisolation. A sample was treated with *COX1*$^{1-19}$. Samples were analyzed by western blotting. Total, 0.4%; eluate, 100%.

(D and E) Purified mitochondria from HEK293T uL1m^{FLAG} cells were treated *COX1*$^{1-19}$ (D) or *COX2*$^{1-23}$ (E). Then, mitochondrial ribosomes were immunoisolated with anti-FLAG beads. Mitochondrial mRNA abundance in eluates were analyzed by nanoString technology. The results are presented as fold change to the non-treated uL1m^{FLAG} control (dashed line) (mean ± SEM; n = 4 or n = 3, respectively).

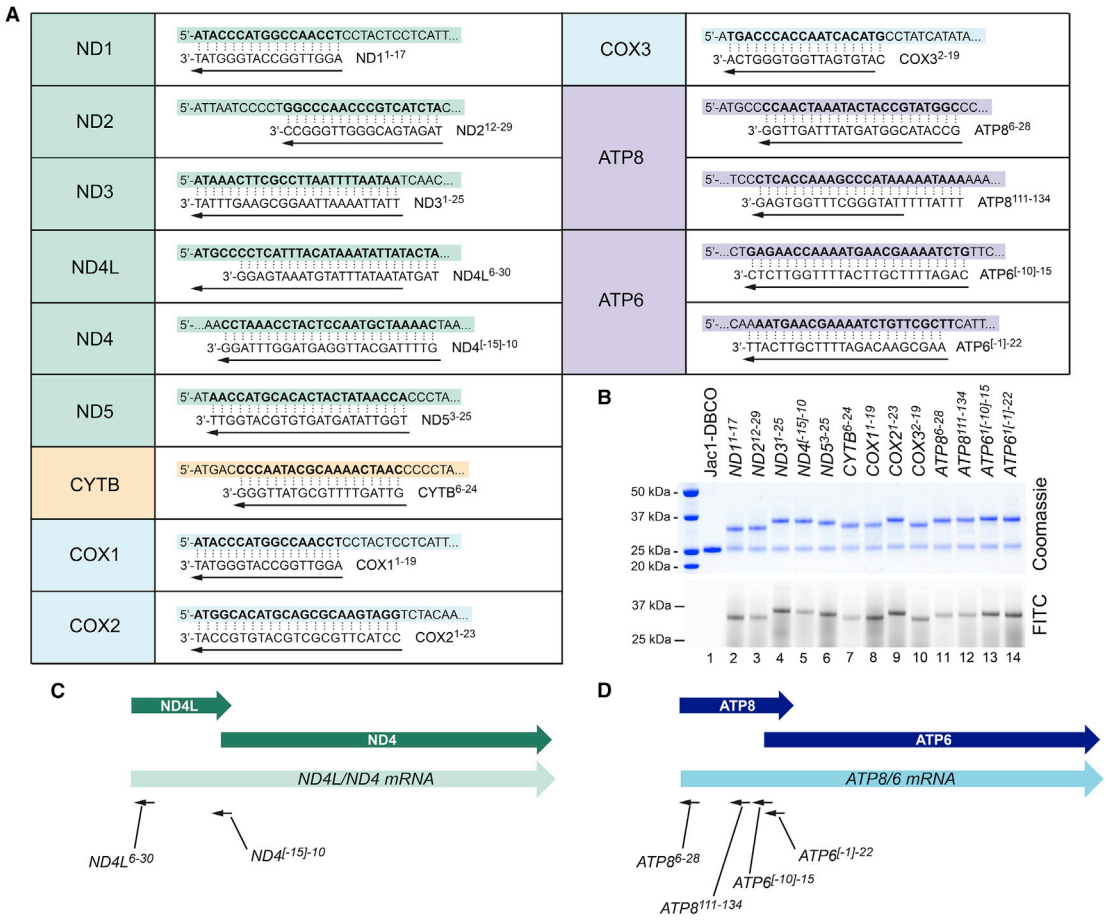

Figure S3. Design and synthesis of chimera targeting translation, related to Figure 3

(A) Schematic presentation of morpholinos targeting mitochondrial mRNAs. Targets are grouped according to OXPHOS complexes.

(B) Synthesis of the precursor-morpholino chimeras targeting to human mitochondrial transcripts used in this study.

(C and D) Schematic presentation of bicistronic mRNA coding for ND4L and ND4 (C) or ATP8 and ATP6 (D). Both open reading frames (ORF) (dark green or dark blue) overlap in the coding sequence (light green or light blue). The approximate binding positions of the chimera tested are depicted as small arrows.

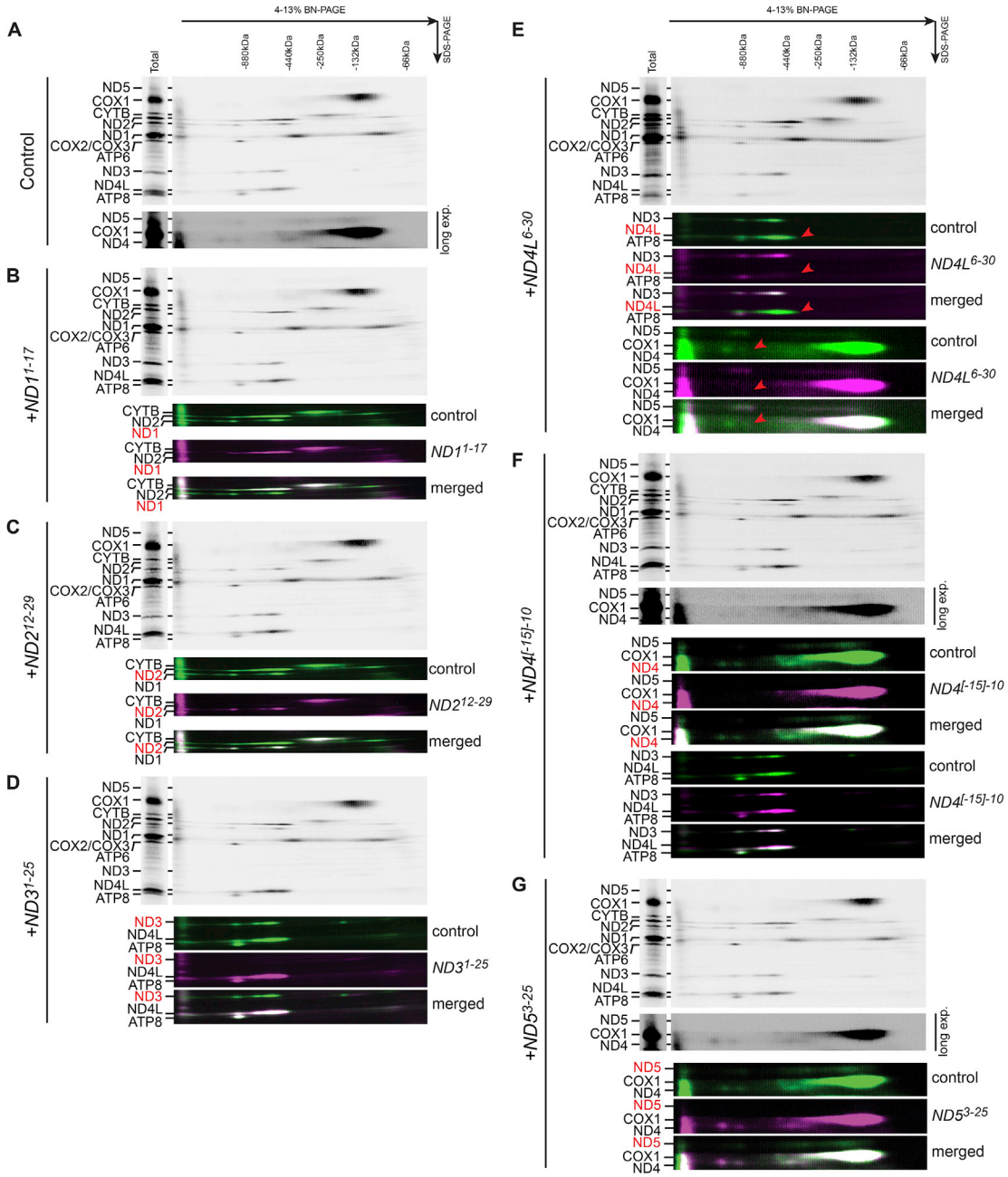

Figure S4. Inhibition of complex I subunit synthesis, related to Figure 3

(A) 1st dimension BN-PAGE followed by 2nd dimension SDS-PAGE (2D) analysis of control HEK293T mitochondria.

(B–G) Downregulation of the synthesis of complex I subunits ND1 (B), ND2 (C), ND3 (D), ND4L (E), ND4 (F), and ND5 (G). False colored sections, including the targeted proteins, are presented and merged with the same region from the control. Targeted proteins are highlighted in red. In (E), ND4L signal is indicated with a red arrowhead.

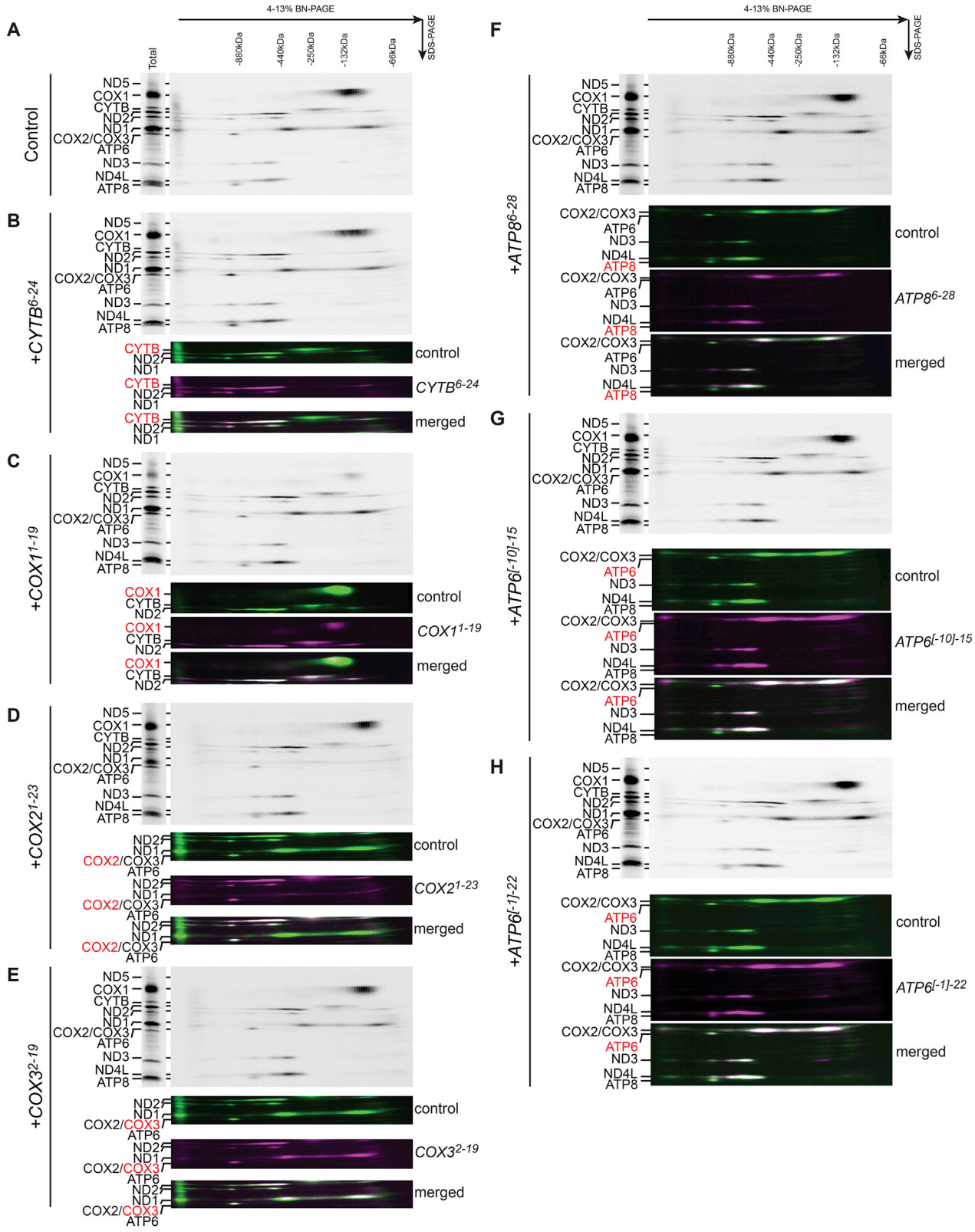

(legend on next page)

Figure S5. Inhibition of complex III, complex IV, and complex V subunit synthesis, related to Figure 3

(A) 1st dimension BN-PAGE followed by 2nd dimension SDS-PAGE (2D) analysis of control HEK293T mitochondria (same as in Figure S4A).

(B) Downregulation of the CYTB synthesis (complex III).

(C–E) Downregulation of the synthesis of complex IV subunits COX1 (C), COX2 (D), and COX3 (E).

(F–H) Downregulation of the synthesis of complex V subunits ATP8 with ATP8$^{6\text{-}28}$ (F), and ATP6 by using two different morpholinos, ATP6$^{[-10]\text{-}15}$ (G), and ATP6$^{[-1]\text{-}22}$ (H). False colored sections, including the targeted proteins, are presented and merged with the same region from the control. Targeted proteins are highlighted in red.

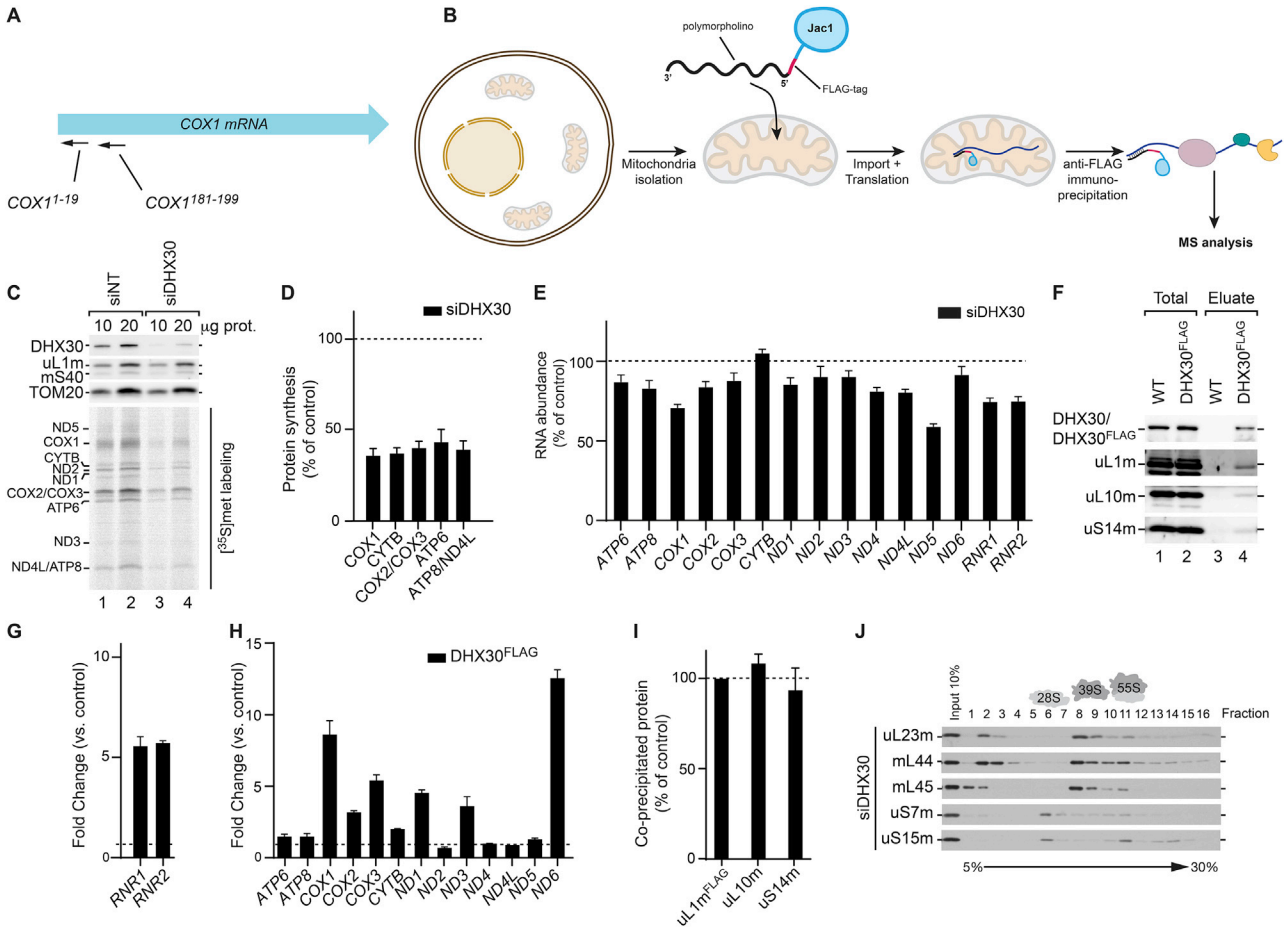

Figure S6. Role of DHX30 in mitochondrial function, related to Figures 4–6

(A) Schematic presentation of *COX1* mRNA and relative binding sites of COX1$^{1-19}$ and COX1$^{181-199}$.

(B) Experimental strategy for morpholino-based mRNA immunoisolation and mass spectrometric analyses (MS).

(C) Mitochondrial translation products were labeled with [^{35}S]methionine in cells after siRNA treatment. Non-targeting siRNA (siNT) was used as a control.

(D) Quantification of [^{35}S]methionine-labeled mitochondrial translation products from (C), percent of siNT control (dashed line) (mean ± SEM; n = 3).

(E) Mitochondrial RNA abundance was determined by nanoString technology in DHX30-depleted cells (mean ± SEM; n = 4). RNA abundance presented as % compared to WT control (dashed line)

(F) DHX30^{FLAG} was immunoisolated from purified mitochondria and samples analyzed by western blotting with indicated antibodies. Total, 5%; eluate, 100%.

(G and H) nanoString technology was used to assess enrichment of mitochondrial ribosomal RNAs (G) and (H) mRNAs in the immunoisolated fractions from (F) (mean ± SEM; n = 4). Dashed line, control values.

(I) Mitochondrial ribosomes were isolated from purified mitochondria after siRNA-mediated downregulation of DHX30 via uL1m^{FLAG} immunoisolation. Samples were analyzed by western blotting. Signal intensities were quantified, normalized to the bait (uL1m^{FLAG}), and are displayed as percent of the control (mean ± SEM; n = 3).

(J) DHX30-depleted mitochondria were analyzed by sucrose density gradient analyses to separate mtSSU (28S), mtLSU (39S), and monosome (55S). The siNT control is displayed in Figure 6E.